UNIVERSITY OF OKLAHOMA GRADUATE COLLEGE

Impact of Vortex Generators on Archimedes Spiral Wind Turbine

A THESIS

SUBMITTED TO THE GRADUATE FACULTY

in partial fulfillment of the requirements for the

Degree of

MASTER OF SCIENCE

By

Joseph Yun

Norman, Oklahoma

2025

Impact of Vortex Generators on Archimedes Spiral Wind Turbine

A THESIS APPROVED FOR THE

SCHOOL OF AEROSPACE AND MECHANICAL ENGINEERING

BY THE COMMITTEE CONSISTING OF

Dr. Srikanth Bashetty, Chair

Dr. Yingtao Liu

Dr. Wilson Merchan Merchan

Abstract

This research presents a novel method for studying the effect of vortex generators on an Archimedes Spiral Wind Turbine (ASWT), demonstrating improvements in power output and efficiency compared to conventional designs. While many forms of horizontal-axis wind turbines exist, the Archimedes spiral wind turbine is particularly efficient for small-scale applications and performs well at low wind speeds. The design features three blades characterized by a uniform spiral growth. Vortex generators (VG) are small devices that enhance flow attachment by creating vortices. This study explores the potential benefits of integrating vortex generators with ASWTs to enhance Horizontal Axis Wind Turbine (HAWT) systems and applications. Computational Fluid Dynamics (CFD) simulations were conducted to assess and compare the effects of these generators on the ASWT. The CFD analysis was performed using the Reynolds-Averaged Navier-Stokes (RANS) equations through the FLUENT package of ANSYS. Initial results showed that large vortex generators negatively impacted performance, reducing efficiency compared to both conventional and small vortex generators because the large vortex generators introduced unwanted drag. Conversely, the inclusion of small vortex generators increased power output by 3.3%, 2.4%, 0.5%, 1.7%, and 4.7% at Tip Speed Ratios (TSR) of 1.0, 1.5, 2.0, 2.5, and 3, respectively. Subsequently, an experiment was conducted to assess the effect of VGs on both modified and conventional systems. The results measured at frequencies of 6, 8, 10, 12, 14, 16, 18, 20, 22, and 24 Hz, indicated changes in output of -12.5%, -12.5%, 0%, 6.1%, 7.0%, 0.6%, 2.3%, 0.2%, 4.2%, 4.2% respectively. Overall, it was concluded that power output is enhanced at higher TSRs, confirming that vortex generators improve the performance of the ASWT.

Table of Contents

List of Figures

List of Tables

List of Acronyms

TSR – Tip Speed Ratio

FVM – Finite Volume Method

ASWT – Archimedes Spiral Wind Turbine

HAWT – Horizontal Axis Wind Turbine

VAWT – Vertical Axis Wind Turbine

MRF – Multiple Reference Frame

SST – Shear Stress Transport

C_p – Rotor Power Coefficient

C_T – Rotor Torque Coefficient

D – Rotor Diameter

RANS – Reynolds Average Navier Stokes

VG – Vortex Generator

RPM – Rotation Per Minute

Chapter 1 Introduction

1.1 Motivation

Wind energy technology has significantly advanced due to the increasing demand for renewable and sustainable energy sources worldwide. Concerns about climate change and environmental degradation continue to grow due to the excessive amount of greenhouse gas output from human activities. These activities include utilizing gas cars, burning fossil fuels, and the destruction of forests [1]. Therefore, the need for clean energy solutions has become a more critical matter. Wind energy is abundant, and capturing clean energy using turbines is one of the most practical and viable alternatives to replace fossil fuels [2]. Capturing wind energy through turbines has become a key strategy for reducing greenhouse gas emissions. However, enhancing the performance of wind turbines remains a crucial area of research, as it directly impacts the viability and scalability of wind power generation. Small-scale wind turbines benefit the environment because they are cost-effective and safe for the environment around them [3]. There are concerns that the traditional horizontal-axis wind turbines kill birds and potentially affect wildlife [4]. The small-scale wind turbine reduces the number of birds affected by the turbine.

One of the common types of small turbines is called the Archimedes Spiral Wind Turbine (ASWT). The design of this turbine is inspired by the Archimedean spiral principle and unlike traditional wind turbines that rely on lift-based aerodynamics, the ASWT uses both the lift and drag forces to generate torque [5]. Figure 1 shows the three blade parameters to help develop an ASWT that leads to the overall development of the turbine.

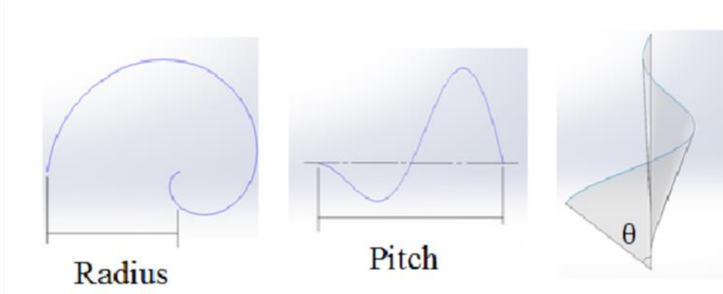

Figure 1: Blade Parameters [6]

In some locations where large wind turbines are not practical, implementing an ASWT is a great alternative to a clean and effective renewable energy source [6]. Wind turbines convert wind kinetic energy into mechanical power, which is then transformed into electrical power using generators [7]. The aerodynamic performance of the turbine blades plays a critical role in the efficiency of this energy conversion process. Managing flow separation and turbulence in wind turbine design is an ongoing challenge, as these factors can lead to significant energy loss. When airflow separates from the surface of the blade, it creates turbulent regions that increase drag and reduce the overall aerodynamic efficiency of the turbine [8]. Additionally, flow separation can lead to dynamic stalls, further diminishing the effectiveness of the turbine in harnessing wind energy.

To address these challenges, extensive research has been conducted to improve the overall performance of wind turbines. Vortex generators (VGs) have been incorporated into wind turbines and aircraft to improve their performance. Figure 2 shows the implementation of vortex generators on a traditional wind turbine, highlighting the placement of the vortex generators.

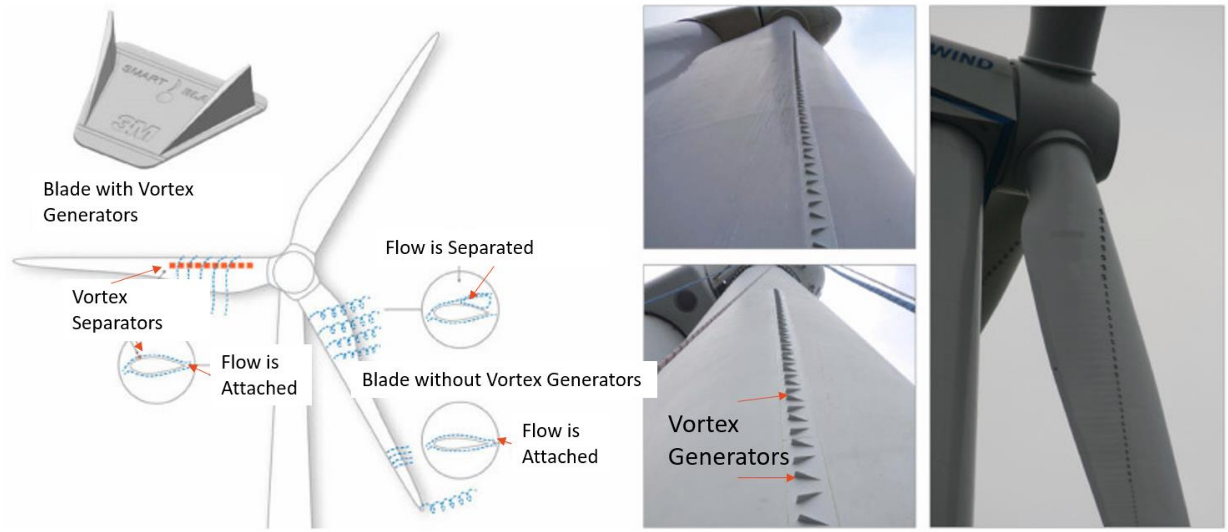

Figure 2: Application of Vortex Generators [8]

Vortex generators are small and placed at the most optimized locations to assist in regulating airflow over the turbine blades. VGs help create localized turbulence that keeps the flow attached to the blade surfaces and are implemented to help mitigate the soiling-induced separation. The delay in flow separation helps to reduce drag and increase lift, resulting in enhancing the wind turbine performance [8].

1.2 Objectives

The main goal of this research is to study the effects of vortex generators on an Archimedes spiral wind turbine to enhance power output. To achieve the goal, an objective list has been created.

1. Design accurate models of both the Conventional and Modified ASWT using suitable modeling techniques.
2. Utilize Computational Fluid Dynamics (CFD) to simulate airflow and aerodynamic characteristics for both ASWT models.

3. Design and execute experimental tests to evaluate performance differences between the Conventional and Modified ASWT under controlled conditions.
4. Assess how the addition of vortex generators impacts aerodynamic efficiency, turbulence characteristics, and overall system performance.

Major work and analysis have been done in Chapter 3. The remaining chapters build upon previous findings by exploring different methods in greater depth. This work is organized as follows: Chapter 1 introduces the motivation and objectives of the research. Chapter 2 introduces background research and initial findings. Chapter 3 presents an extension of the IEEE Greentech conference paper that details the simulation and experimentation with vortex generators (VGs) on the Archimedes Spiral Wind Turbine (ASWT) that will later be published in a journal. Chapter 4 discusses the results and provides a thorough discussion of the findings, and Chapter 5 offers a conclusion based on the research of the simulation and experimental results.

Chapter 2 Background Research

The use of vortex generators on wind turbines has been studied by Bahador [9]. This paper highlights the mechanism of slot and vortex generator treatment in the transitional boundary layer. Research found that the lift-to-drag coefficient increased to 112% at 16.3 degrees when compared to the uncontrolled case. However, the coefficient performance decreases to an average of 12.3% for pre-stall angles. The study utilizes the Ansys-Fluent v18.2 software using the time-dependent implicit algorithm implemented to Reynolds Averaged Navier-Stokes. The turbulence model used in their simulation was $\gamma - \overline{Re_{\theta t}}$. This turbulence model was used for its ability to capture the transient characteristics of the flow separation and the boundary layer needed to accurately model the turbulence. This turbulence model is a new correlation-based transition model that is based solely on local variables [10]. Where γ is the intermittency and $\overline{Re_{\theta t}}$ is the Momentum Thickness Reynolds Number.

Research by Hyeongi Moon [11] indicated that implementing a vortex generator on a MW-class wind turbine blade plays a role in helping suppress the dynamic load and delay flow separation and aerodynamic stalling. To validate the vortex generators' impact on the performance of the windmill, vortex generators were installed on the 2.3 MW wind turbine blades. The Aerodynamic performance data was collected in the span of 2 months, utilizing the Supervisory Control and Data Acquisition system, and compared to that of the same MW wind turbine without the vortex generator. Analysis shows that at high wind speeds, vortex generators perform better and improve power generation. However, it was found that at lower speeds, it tends to underperform. The Moon experiments resulted in a 2.8% increase in power generation at a rated wind speed of 10m/s. This study only emphasized a specific VG design and placement. Further research can be conducted to explore the optimization of Vortex generator shapes, sizes, and placement to maximize performance.

Additionally, a study conducted by Ruifang Jiang [12] explored the effects of vortex generators on wind turbines while considering rotational effects, using the inverse blade element moment method to compare output torque and pressure coefficient values with and without vortex generators. This experiment utilized the $\gamma - Re_{\theta t}$ transition model, Phase VI wind turbine rotating blade, and simulating the airfoil of S809. Phase VI is a reference to specific research conducted by the National Renewable Energy Laboratory in collaboration with NASA [13]. The characteristic and flow field structures were analyzed using the same Reynolds number (Re) to investigate the three-dimensional rotational effect. A comparison was conducted to compare the flow fields of each blade section with and without the vortex generators. By conducting the simulation, it was found that the three-dimensional rotational effect was most prominent at the blade roots. By placing vortex generators in the area enhanced the effect by increasing the C_L by 4.4% and 0.6% at 10 m/s and 13 m/s respectively. It was also found that the vortex generators increase the turbine torque output by 3.73%, 8.74, and 10.82% at wind speeds of 10, 13, and 15 m/s, respectively.

The research conducted by Im focuses on the role of vortex generators in enhancing the performance of wind turbine blades by preventing premature stalling in the inboard region [14]. It was stated that it is important to prevent premature stalling for stability and power generation. As blade length increases, airfoils with higher thickness-to-chord ratios are needed to manage increased root area loads, but this can lead to premature stalling and radial flow losses. VGs address this by stabilizing the boundary layer and preventing flow separation, thereby eliminating the need for complex control systems. The study uses computational fluid dynamics (CFD) simulations to assess various VG placements, revealing that optimized VG placement can increase annual energy production by 1.48% to 1.63%, depending on average wind speeds. The proposed VG design criteria, developed for airfoils at the maximum chord length position, help mitigate power losses caused by environmental and stability issues, offering a significant improvement in rotor performance and turbine efficiency. This research utilized the Rigid Body Motion method of STAR CCM+ v15.04 (Siemens) and the turbulence model k-ω SST gamma-Re-θ model.

Horizontal axis wind turbines (HAWT) come in many sizes and types and have undergone optimization in the wind turbine industry. Gianluca Zitti conducted experiments with a screw-shaped Archimedes spiral [15]. This design aims to create a new type of hydrokinetic turbine while minimizing costs and maintaining environmental friendliness. A more common small-scale turbine is the Archimedes spiral type, and research was focused on improving its power output and efficiency by analyzing different spiral sizes and blade shapes.

A study by Mohammed was conducted on two Archimedes Spiral Wind Turbine (ASWT) rotor designs (fixed angle and variable angle) to determine the optimal performance [16]. This type of turbine benefits from the advantages of a low-speed axial flow turbine. The study involved both numerical and experimental analyses, where numerical simulations were used to predict turbine performance under various conditions with the use of ANSYS Fluent and MRF, and experimental measurements were conducted to validate the results in the simulation. It was found that by comparing the two designs, the variable-angle rotor performs better than the fixed-angle rotor. The results show that power and torque coefficients increase with rising wind velocity in both designs. However, the variable-angle design achieves a 14.7% higher power output compared to the fixed-angle design.

In the study by Abdel, to further boost the output power of the Archimedes spiral, external methods were used. One such as, using an optimized shroud to concentrate flow to a specific area, has resulted in a power coefficient increase of 2.58 times compared to the Archimedes spiral without an optimized shroud [17]. This study enhances ASWT performance by optimizing a shroud design featuring an inlet flange, aiming to maximize the power coefficient (Cp). The optimization process employs an Evolutionary Algorithm in conjunction with a Kriging interpolative model. A set of straight lines is used to define the shroud’s shape. The Cp is determined by solving the Reynolds-averaged Navier-Stokes (RANS) equations with the SST k-Ω turbulence model using ANSYS-FLUENT commercial software.

Before determining the best size that improves the power output, a large vortex generator has been initially considered and shown in Figure 3. The vortex generators are arranged in a straight configuration and have 3 pairs of VG’s on each blade.

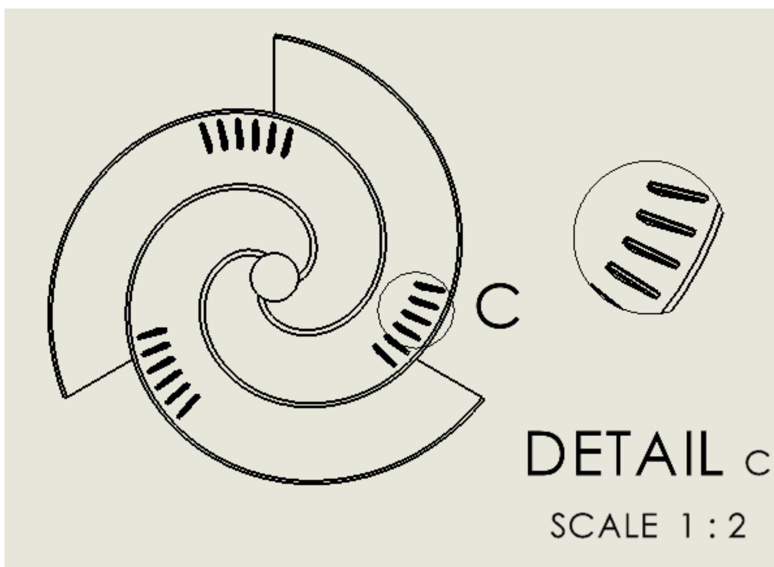

Figure 3: ASWT with large vortex generators

Different sizing and orientation have been conducted to find the most effective placement of the VG’s. The VGs are placed perpendicular to the blades' outer rim of the blade and equal distance from each VG. The sizing of the larger VG is about 5 times larger than the smaller vortex generator designed in Chapter 3. The potential negative about having a large vortex generator is that it may introduce unwanted drag. Figure 4 shows the dimensions used to create the vortex generators. Designing the right size is crucial and can be further studied in the future.

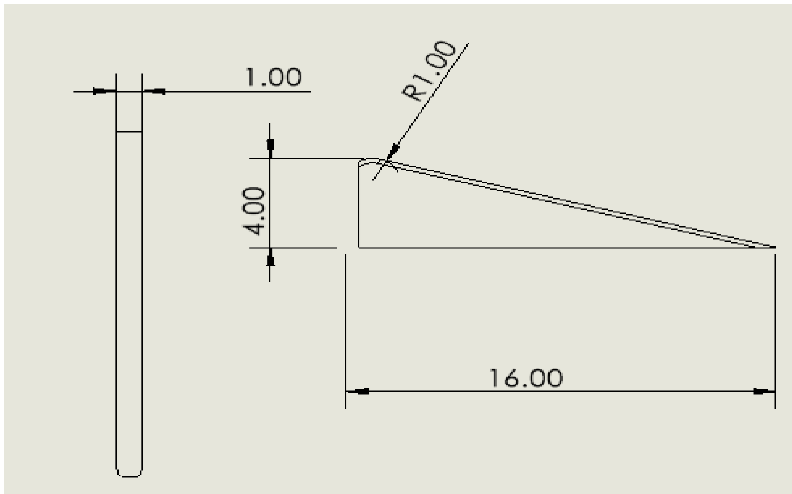

Figure 4: Dimensions (mm) of Larger Vortex Generator

2.1 Simulation Methods

Dynamic meshing in Ansys Fluent was attempted to simulate real-time interaction with the blades. Dynamic mesh requires high-cost computational power to simulate the blades' structural deformation and rotational effect. It is utilized when the simulation involves moving or deforming boundaries that cannot be handled in a static mesh [18]. It is a transient case where the timestep is a factor and can simulate the sequence of the fluid-structure interaction. However, this method was found to have high computational cost, and the time to calculate was too long compared to a steady-state simulation. Dynamic mesh often led to divergence errors and was found to be unnecessary for this study, as steady state calculations exist using Multiple Reference Frames (MRF). Dynamic meshes are more suitable in applications such as Aeroelastic simulation, droplet interaction, or wave impact on structures.

The use of Ansys CFX 2024 has been attempted as well. This method is similar to Ansys Fluent; however, Fluent offers more advanced turbulence models, such as SST k-ω, LES, and DES, that can better capture these effects. CFX is great for turbomachinery applications, however, Ansys Fluent is great in a lot of broader areas and has a wide application. This study utilizes the multiple reference frame and SST k-ω; therefore, CFX was not chosen for this study [15,16, 17].

The selection of the turbulence model was also considered. The two most common turbulence models are SST k-ω and Realizable k-ε. The strength of the k-ε is that it performs well in the far-field and free-stream regions where turbulence has been fully developed. It is also good for external aerodynamics; however, this turbulence model performs poorly near-wall performance due to its reliance on wall function and struggles with strong adverse pressure gradients and flow separation [10]. In this model, a Y+ <30 is suitable for accurate results. On the other side, the SST k-ω turbulence model performs well near the wall region, which is important for simulating boundary layer flows. This model is also more accurate for flows with separation and adverse pressure gradient and is more stable in low Reynolds numbers. This model is weak in free-shear or fully developed turbulence compared to that of k-ε, but it can automatically switch between k-ω and k-ε. Since this study involves flow separation, boundary layers, and wall interaction, the k-ω is the most suitable model.

Chapter 3 Harnessing the Wind: Evaluating Vortex Generators on Archimedes Spiral Turbines

3.1 Introduction

Wind energy technology has advanced substantially in response to the global push for renewable and sustainable energy. There have been increasing worries about climate change and environmental damage, which emphasize the urgent need for clean energy solutions. Among available options, wind power is especially appealing because wind resources are abundant and available in many areas [19]. Turbine-based energy capture is both practical and effective for replacing fossil fuels while being less harmful to the environment. Harnessing wind energy through turbines therefore stands out as a key strategy for cutting greenhouse gas emissions [2]. At the same time, improving turbine performance remains an essential area of research, as it profoundly influences the feasibility and scalability of wind power. Small-scale wind turbines offer environmental advantages by being able to be implemented in urban and populated areas [3]. It is also found that MW turbines have an impact on their surroundings, such as producing noise and disrupting birds [4].

In order to generate power, wind turbines are designed to capture moving air to transform the kinetic energy into mechanical power [7]. However, optimizing this process focuses on managing the aerodynamics of the blades. Flow separation and turbulence can significantly undermine energy production since they increase drag and reduce efficiency. When airflow detaches from the blade surface, it forms turbulent zones that degrade aerodynamic performance, leading to dynamic stalls and further impairing the turbine's ability to capture wind energy effectively [12].

In response to these challenges, researchers have devoted considerable effort to enhancing wind turbine performance. One innovation is the use of vortex generators (VGs), which have also shown effectiveness in aircraft applications and automobiles [20]. Because VGs are small, they can be strategically placed at optimal points along the blade surfaces to control airflow [11]. By inducing localized turbulence, these devices help maintain attached flow and reduce soiling-induced separation. As a result, airflow detachment is delayed, lowering drag and increasing lift outcomes that improve the turbine's overall power output [9].

VGs are implemented to help mitigate the soiling-induced separation. Blade soiling was found a 6.6% reduction in Annual Energy Production for the NREL 5-MW wind turbine and was able to transform into a 1% increase through the application of VGs mentioned by Tian [1]. This paper provided quantitative results to be used to optimize the layout of a wind turbine. Research by Hyeongi Moon [11] indicated that implementing a vortex generator on a MW-class wind turbine blade plays a role in helping suppress the dynamic load and delay flow separation and aerodynamic stalling. Moon's experiments resulted in a 2.8% increase in power generation at a wind speed of 10m/s. Additionally, a study conducted by Ruifang Jiang [12] explored the effects of vortex generators on wind turbines while considering rotational effects, using the inverse blade element moment method to compare output torque and pressure coefficient values with and without vortex generators. Research by Yangjiang Yang studied the aerodynamic enhancement for HAWT with vortex generators [21]. In this study they found that at TSR 5.83, the vortex generators increase the coefficient of power by 47.8% under rough wall condition. The study found that VG reduced the negative impacts of blade surface roughening on aerodynamic performance.

Horizontal axis wind turbines (HAWT) are produced in a variety of sizes and designs, reflecting ongoing optimization efforts within the wind energy sector. An example is the screw-shaped Archimedes spiral turbine, which Gianluca Zitti [15] investigated with the goal of creating an economical and eco-friendly hydrokinetic system. At smaller scales, the Archimedes spiral type remains a popular choice, with research frequently targeting improvements in blade geometry and spiral dimensions to enhance power production and overall efficiency. One study on the blade design of the Archimedes turbine found that a variable-angle rotor yielded a 14.7% increase in power compared to a fixed-angle design [16]. To further boost the output power of the Archimedes spiral, external methods, such as using an optimized shroud to concentrate flow to a specific area, have resulted in a power coefficient increase of 2.58 times compared to the Archimedes spiral without an optimized shroud [17]. A numerical aerodynamic analysis of the ASWT was conducted by Sahand Ebrahim. Using the turbulence model SST k-ω and using ANSYS CFX, they conducted two numerical analyses [22]. The study first simulated and calculated the 0.5kW ASWT model. They then scaled down the model to 1:10 and validated the numerical results. They found that, with the turbine diameter of 1.5 m, the maximum power coefficient is obtained at TSR 2.5. Ozeh's study covers a variation of the ASWT with the blades being 120 degrees from each other. The design was then 3D printed and experimented with by attaching it to a DC motor placed into the wind tunnel to measure voltage and power. This study found that at TSR 1.48 with a wind speed of 4 m/s, it performed the best [23].

In this study, the objective is to develop a model that enhances power output by utilizing vortex generators and comparing the results of the conventional and modified ASWT through both simulation and experimentation. The remainder of the paper is organized as follows: Section 3.2 describes the model used and the governing equations for the simulation. Section 3.3 explains the meshing process of the model, the boundary conditions, and the simulation results to accurately simulate the turbine's interaction with wind velocity. Section 3.4 shows the experimental process and setup. The conclusions and suggestions for future work are presented in Section 3.5. This chapter extends the paper presented at IEEE GreenTech conference and will be published in a journal.

3.2 Mathematical Modeling

To achieve an accurate aerodynamic pattern and a precise model of the flow, it is essential to select the appropriate turbulence model. The Reynolds Average Navier-Stokes (RANS) equations are used to estimate fluid motion and flow behavior. Flow is considered incompressible if the Mach number is less than 0.3, in which case it will only depend on the velocity term in Equation 1. The pressure can be determined from the momentum equation, as shown in Equation 2. By utilizing discrete quantities from both the continuity equation and the momentum equation, we can obtain the pressure.

Continuity equation:

$$\frac{\partial \overline{U_i}}{\partial x_i} = 0 \qquad (1)$$

Momentum Equation:

$$\frac{\partial \bar{U}_i}{\partial t} + \frac{\partial (\bar{U}_i \bar{U}_j)}{\partial x_j} = -\frac{1}{\rho}\frac{\partial \bar{p}}{\partial x_i} + \nu \frac{\partial^2 \bar{U}_i}{\partial x_i x_j} - \frac{\partial (U_i' U_j')}{\partial x_j} \qquad (2)$$

Here, $\bar{U}_i$ *and* $\bar{U}_j$ represent the velocity vectors represent the i and j directions, respectively. The term p denotes the fluid pressure, ρ represents the air density, and ν refers to the kinematic viscosity of the fluid. The Cartesian axes are defined as i, j = 1, 2. The mean velocity component is represented by $\bar{U}_i$, while x_i denotes the Cartesian coordinate corresponding to the length in the i-direction. The term $\bar{U}_i \bar{U}_j$ is referred to as the Reynolds stresses, arising from the fluctuations of the associated fluid particles. Studies have shown that the Shear stress Transport (SST) k-ω turbulence model is applicable for performance near the wall boundary, fluid flow separation, and pressure gradients [10]. The SST k-ω turbulence model utilizes the strengths of both k-e and k-ω. Where k represents the energy contained in turbulent eddies, e is the rate of dissipation of turbulence dissipated into thermal energy, and ω measures the rate of dissipation of turbulence kinetic energy per unit turbulence kinetic energy.

Shear Stress Transport k-ω:

$$\frac{\partial(\rho k)}{\partial t} + \frac{\partial(\rho k\, U_{\mathrm{i}})}{\partial x_{\mathrm{i}}} = \frac{\partial}{\partial x_{\mathrm{j}}}\left[\Gamma_{\mathrm{k}} \frac{\partial k}{\partial x_{\mathrm{j}}}\right] + G_{\mathrm{k}} - Y_{\mathrm{k}} + S_{\mathrm{k}} \tag{3}$$

$$\frac{\partial(\rho \omega)}{\partial t} + \frac{\partial(\rho \omega\, U_{\mathrm{i}})}{\partial x_{\mathrm{i}}} = \frac{\partial}{\partial x_{\mathrm{j}}}\left[\Gamma_{\omega} \frac{\partial \omega}{\partial x_{\mathrm{j}}}\right] + G_{\omega} + D_{\omega} - Y_{\omega} + S_{\omega} \tag{4}$$

As mentioned in the equation above Γ_{k} and Γ_{ω} shows the effective diffusivity of k and ω.

$$\Gamma_{\mathrm{k}} = \mu + \frac{\mu_{\mathrm{t}}}{\sigma_{\mathrm{k}}} \tag{5}$$

$$\Gamma_{\omega} = \mu + \frac{\mu_{\mathrm{t}}}{\sigma_{\omega}} \tag{6}$$

G_{k} represents the generation of turbulence kinetic energy due to the mean velocity gradient, and G_{ω} represents the generation of the term ω. The third term on the right side of the Eq. (3) Y_{k}, is the dissipation of k, while in Eq. (4) Y_{ω} represents the dissipation of ω. The last term on the right side of Eq. (3) S_{k}, represents the production of turbulent kinetic energy to the strain rate of the mean flow and the for Eq. (4), S_{ω} represents the source term for the specific dissipation rate ω In Eq. (5) and Eq. (6), μ is the molecular dynamic viscosity, μ_{t} represents the turbulent eddy viscosity,

σ_k and σ_ω are the turbulent Prandtl numbers for k and ω. Eq. (5) and Eq. (6) describe how the transport properties of k and ω are affected by both molecular and turbulent viscosity.

3.2.1 ASWT Design and Geometry

The design of the ASWT was referenced according to Nawar [16]. This design consists of a 250 mm diameter with an angle of 120 degrees. SolidWorks 2024 is used to construct a 3D model of the ASWT shown in Figure 5, Figure 6, and Figure 7. The blades have a thickness of 3 mm, and the rotor diameter is 25 mm. This research created a conventional Archimedes spiral wind turbine according to the features in Table 1.

Table 1: Archimedes Spiral Wind Turbine Design Parameters

Parameter	**Value**
Nominal Thickness (t)	3 mm
Length (L)	218 mm
Diameter (D)	250 mm
Inner Diameter (d)	25 mm
Fixed-Pitch (P)	101 mm

As shown in Table 1, the parameters were created to maintain consistency throughout this study. The conventional and modified Archimedes spiral wind turbine will follow this base design. This is to ensure that only the vortex generator affects the blade's performance. Figure 5 provides the dimensions of the turbine that was modeled in SolidWorks. Displayed from left to right are the front view, side view, and cross-section of the turbine.

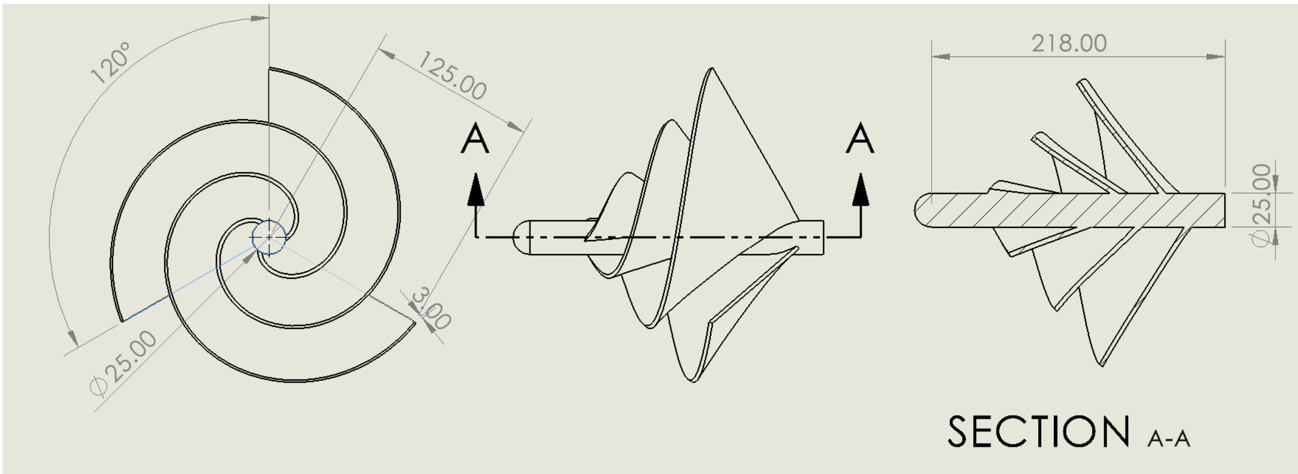

Figure 5: SolidWorks Drawing of Unmodified Archimedes Wind Turbine

Figure 6 illustrates the ASWT with the implementation of vortex generators. VGs are placed near the tip of the turbine to ensure they capture the most wind. The vortex generators are evenly spaced throughout the spiral, with a total of 46 instances and 2.6 mm equal spacing.

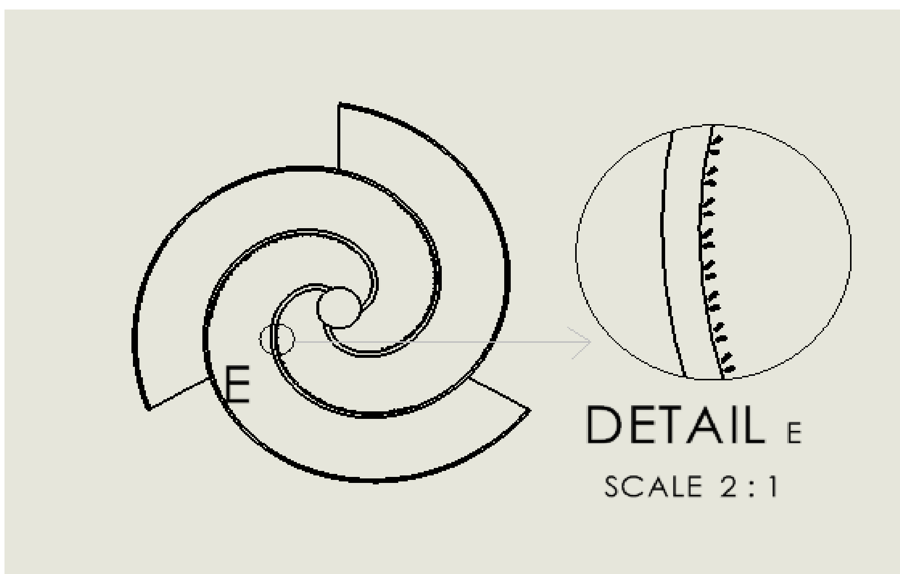

Figure 6: SolidWorks Drawing of Modified Archimedes Wind Turbine

Figure 7 shows the dimensions of the vortex generators used on the ASWT. The angle of 32 degrees was selected based on a previous study [12]. The dimensions of the vortex generators are based on another study [11], where the dimensions are derived from the boundary layer thickness.

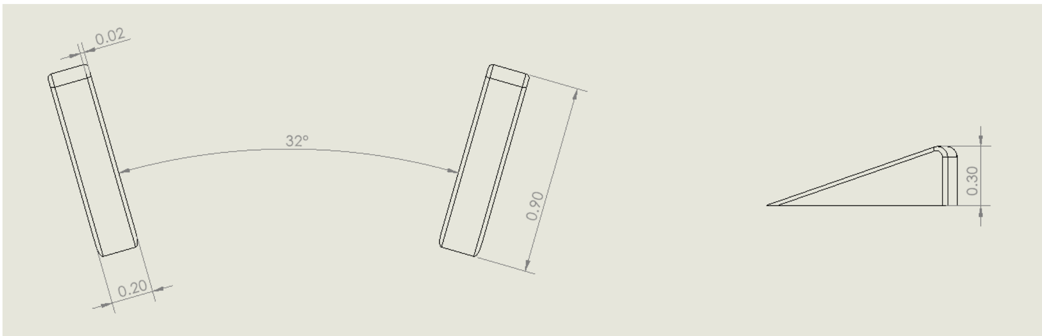

Figure 7: Dimensions of Vortex Generators

These dimensions were chosen to be small to reduce the drag and overall power loss and ensure the condition of a maximum power coefficient. This study focuses on comparing a base ASWT model to a modified ASWT Model. The modified model implements a vortex generator to the ASWT and examines its effect on the performance and flow field.

3.3 Simulation

3.3.1 Setup

After the model had been created in SolidWorks and converted to a STEP file, ANSYS Fluent was utilized to simulate the performance of the Archimedes Spiral Wind Turbine. A force acts on the blades, causing them to rotate due to the drag exerted on the three blades. These small and compact wind turbines are ideal for small applications and can fit into tight spaces. A flowchart is provided to illustrate this process as shown in Figure 8.

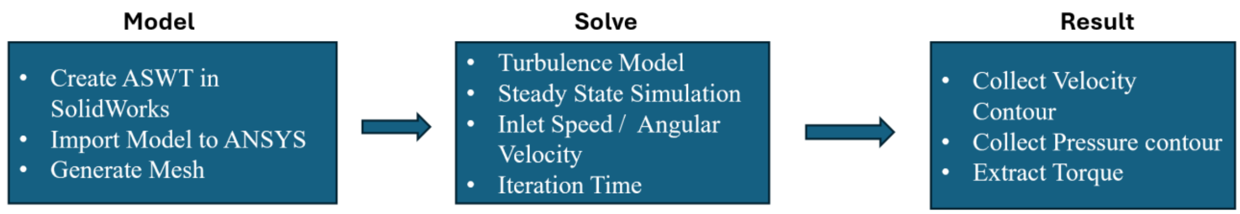

Figure 8: Process Flow Chart

The first step involved checking whether the model had been successfully transferred to the ANSYS DesignModeler software. It was important to ensure that no parts were missing in the solid body. After completing this initial check, the process of volume extraction for the ASWT and the creation of fluid and solid domains began.

3.3.2 Mesh Generation

There are three main regions for this flow simulation: the stationary domain, the rotating domain, and the ASWT. Each region requires a specific mesh size to accurately capture the model while also saving on computational costs.

The rotating domain, which contains the inner dome, is designed to allow the turbine to spin and assess the flow around it. This domain had a smaller mesh size since it is the area of interest where critical values are calculated. In contrast, the mesh size for the stationary domain is larger and contains less detail. The third region, the ASWT, necessitates the finest mesh quality to precisely model turbulence and evaluate turbine performance.

In the meshing setup within Ansys, named selections were utilized to ensure proper configuration. Specifically, the inlet face, outlet face, and turbine wall were designated. The inlet is positioned in front of the Archimedes spiral wind turbine, where the inlet velocity is defined as shown in Figure 9. The outlet is located behind the ASWT, which is where the pressure outlet is situated. The stationary domain extends from the inlet to the outlet and encloses the rotating domain.

The rotating domain contains the volume of the ASWT and rotates at the provided angular velocity. As illustrated in Figure 9, two cylindrical domains were established to represent wind conditions: the outer dome, which serves as the stationary domain, is designed to create a computational domain for the wind tunnel model. This dome measures five times the diameter of the turbine, helping to minimize boundary effects and allowing the airflow to remain undisturbed. The size of this domain is critical for achieving reliable and accurate simulation results regarding flow development and wake effects. The inner dome, measuring 270 mm, is slightly larger than the turbine, enabling the simulation of flow interactions with the blades. This inner dome functions as a rotating domain that allows the turbine to rotate freely. To further optimize the model for computational efficiency, fillets were removed to reduce computing costs.

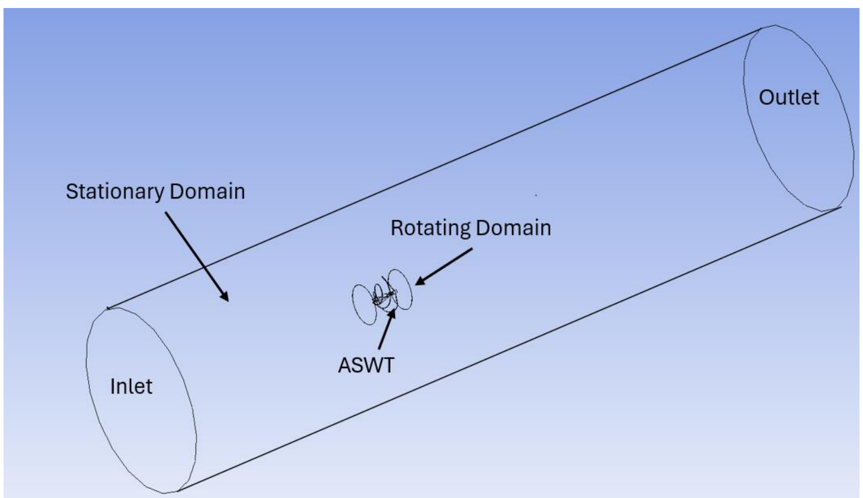

Figure 9: Boundary Condition in Ansys Fluent

The mesh was generated for both domains by applying body and face sizing to the rotating domain while utilizing inflation on the turbine blades. Similarly, face and body size are also applied to the stationary domain. The diameter of the stationary domain is five times that of the turbine. Additionally, the length of the stationary domain in front of the rotating domain is also five times the turbine's diameter, while the length after the rotating domain is eight times the turbine's diameter. The length of the rotating domain is 1.01D as shown Figure 10. The sizing of the domains is to accurately model a wind tunnel where the walls do not affect the inlet wind velocity with the rotating turbine. The length after the rotating domain is longer to capture all the wake regions produced by the rotating turbine. This allows the simulation and contours to be less affected by the outlet by providing enough distance.

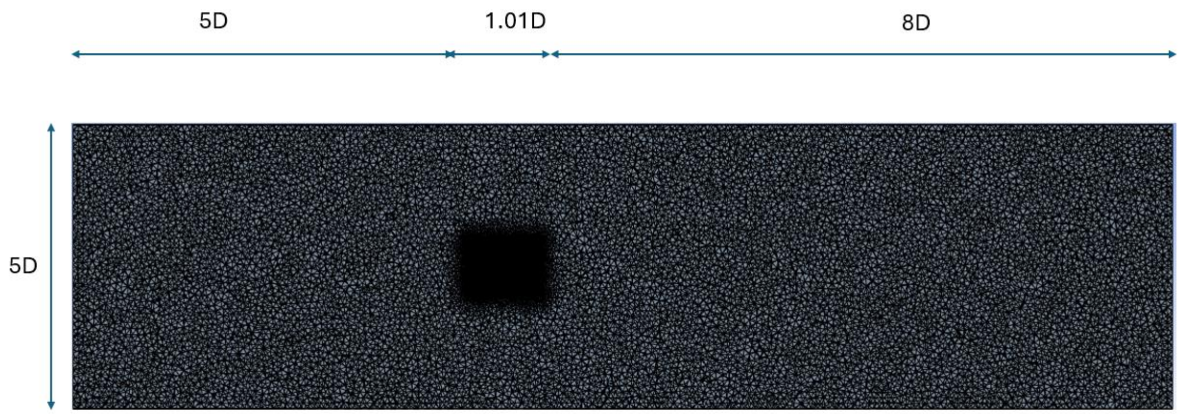

Figure 10: Dimension for Outer Domain The mesh quality was validated through independent mesh study.

Table 2 presents the settings for inflation layers, which refine the results near the wall and improve boundary layer resolution. The mesh quality was validated through independent mesh study.

Table 2: Inflation Settings

Inflation Option	**First Layer Thickness**
First Layer Height	1.3e-004m

Maximum Layers	15
Growth Rate	1.2

For inflation, the first layer height is chosen to be 0.1 mm with a maximum of 15 layers, with a growth rate of 1.2 [16]. A small first layer height resolves near-wall gradients and ensures the y^+<5 condition is met [24] y^+<5 condition is important to improve accuracy in the model and to indicate that the first grid layer is in the laminar sublayer. The growth rate of 1.2 is to avoid abrupt differences in the cell size, as well as ensure a smooth transition and better solve stability. The number of layers is needed to fully capture the boundary layer profile. y^+ is a dimensionless distance with the following Eq. (8)

$$y^+ = \frac{u^* y}{v} \tag{8}$$

Where u^* represents the friction velocity, v is the kinematic viscosity, and y^+ is the distance to the wall. u^* can be found with the following Eq. (9)

$$u^* = \sqrt{\frac{t_w}{p}} \tag{9}$$

t_w represents the wall shear stress and p represents the fluid density. The y^+ value is important in CFD turbulent flow as it determines how well the near-wall turbulence is resolved. With y^+<4, CFD solvers can accurately model the viscous stress, flow detachment, and separation [19][25]. The turbulence model SST k-ω requires a low y^+ value to accurately predict the simulation. When 5<y^+<30, it is in the buffer layer, which is a zone where the transition region between the viscous sublayer and the log-law region is in a turbulent boundary layer. This range is to be avoided because it represents a transition zone where viscous and turbulent effects interact, making it difficult to model correctly and may over or underpredict the result.

After defining all named selections, a mesh independent study was conducted to provide the solution with an accurate model. As seen in Table 3, different numbers of elements have been utilized. The duration of the calculation varied as the mesh size changed. The 9.1 million elements produced the most accurate result without compromising much more computational time compared to the 8 million number of elements.

Table 3: Mesh Independent Study

Number of elements	**Power Coefficient**
9114384	4.035
8828040	3.98
6658847	3.97
2009651	3.91

To compute the flow fields, we implement a Multiple Reference Frame approach, which includes a rotating frame, a stationary frame, and the turbine blade face. a illustrates the inflation layers added to the mesh to ensure accurate results are captured. Figure 11 displays a smooth transition in mesh size from the outer domain (blue) to the inner domain (grey). This is done by having the same face and body sizing of 7 mm. This ensures numerical stability and avoids divergence.

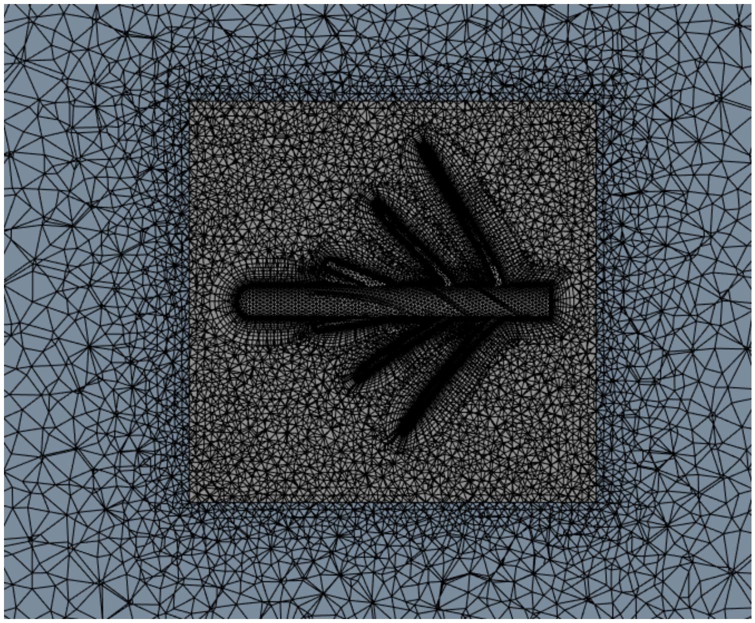

Figure 11: Archimedes Spiral Wind Turbine Mesh with inflation

Figure 12 shows a close-up view of the vortex generator mesh. Visual inspection of the vortex generators is conducted to see if the mesh is fine enough to capture the vortex generators. The view is the turbine with the volume extracted, therefore, there are gaps and holes where the turbine should be.

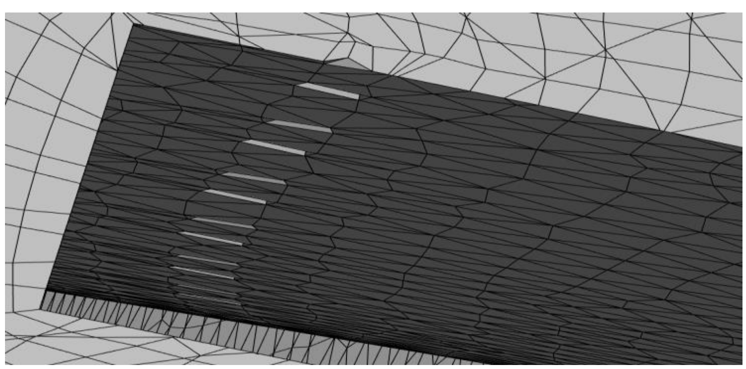

Figure 12: Mesh with Vortex Generators

When all the correct named selections have been placed and the proper selection of mesh size, the model is then transferred over to the ANSYS Setup. As mentioned earlier, the inlet face, outlet face, and turbine wall are named selections to give boundary conditions such as wind speed, pressure, and blade rotational speed respectively.

3.3.3 Boundary Conditions

In ANSYS Fluent, a Double Precision Solver was implemented to improve accuracy for aerodynamic simulations. The domain is defined as a fluid domain consisting of air at a temperature of 25 degrees Celsius and is characterized as a continuous, non-buoyant fluid. The first boundary condition is established at the inlet, where the wind has a normal velocity of 8 m/s, along with corresponding angular velocities for different tip-speed ratios (TSR), setting the turbulence intensity to 5% for a real-world application. For small-scale wind turbines, typical wind operations range from 2 m/s to 15 m/s, therefore, a wind speed of 8 m/s is selected to represent typical wind conditions that small-scale wind turbines may experience. The wind speed is chosen to represent real-world scenarios for residential areas and small-scale wind applications. The walls of the stationary domain are assigned to a no-slip condition. Furthermore, a static pressure difference of zero is set across the outlet to ensure numerical stability. The turbine within the stationary domain also follows a no-slip condition.

After the mesh size has been selected, it is then transferred to ANSYS Fluent as the solver. In the Fluent setup, the inlet flow velocity, outlet pressure, and rotation of the turbine blade are given as the boundary conditions. The cell zone type is set to fluid. Both the inner domain and the turbine walls are set to Frame Motion and given angular velocity. Table 4 shows the model setup parameters.

Table 4: Model Setup Parameter

Parameter	**Description**
Material	Air
Turbulence model	Shear-Stress Transport k-ω
Shape of Domain	Cylindrical
Mesh Type	Hexahedral/Tetrahedral
Inlet	Inlet Velocity (m/s)
Outlet	Pressure Outlet
Residual RMS Criteria	1e-6

The RANS equation was solved using the SST k-ω model and implemented in ANSYS Fluent R2 2024. It is recommended to use the SST k-ω model for flows with high adverse pressure gradients and separation [10]. The cell zone boundary is defined by treating the two domains as separate: the outer domain is considered a stationary frame, while the inner domain is designated as "Frame Motion." Initial values for rotational velocity are provided in the inner cell domain. For the boundary conditions, the inlet velocity was set to 8 m/s. The COUPLED algorithm was used for pressure-velocity coupling, along with second-order pressure, second-order upwind momentum, and turbulent kinetic energy settings for the solution. To ensure convergence, the residual value threshold was set to 10^{-6} as the convergence criterion. The simulation was run for 1500 iterations, during which the reported torque value remained fixed for every 100 iterations. The residual plot shows that the convergence criteria have been met. This plot is used to monitor the convergence of computational fluid dynamics simulations. Residuals indicate the imbalance in a conserved variable within a control volume or represent the error in the solution.

3.3.4 Results

Illustrating the velocity flow and pressure contours can explain the aerodynamic properties and characteristics of both the conventional and modified models of the ASWT. From Figure 13, the tip of the turbine shaft experiences the lowest flow velocity compared to other areas. This increased flow velocity at the tip of the blade generates the torque necessary for the turbine to rotate.

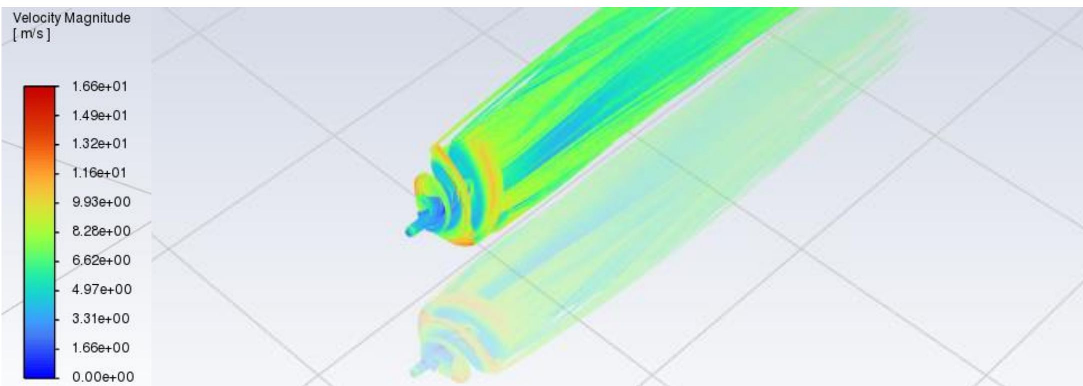

Figure 13: Velocity Flow Field of Conventional Turbine in Ansys Fluent

Figure 14 shows that the pressure difference near the blade tip is higher than in the central region, indicating that most of the energy is concentrated near the tip of the blade, like the horizontal-axis wind turbines.

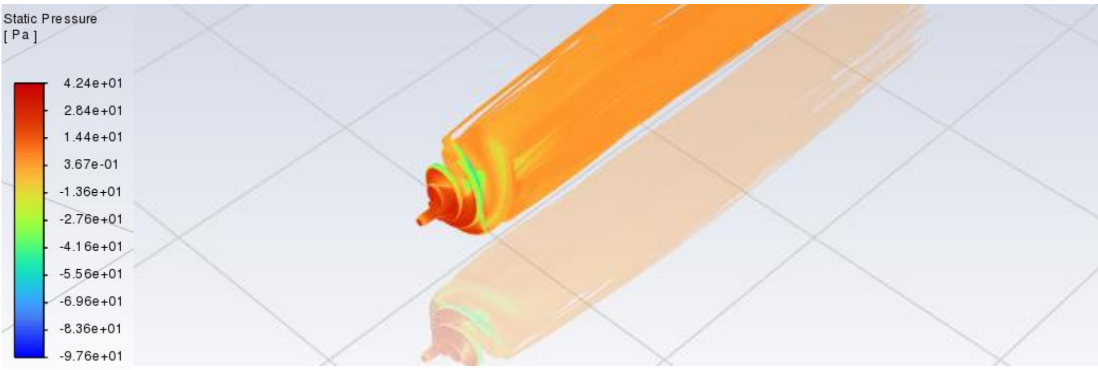

Figure 14: Pressure Flow Field of Conventional ASWT in Ansys Fluent

Figure 15 and Figure 16 are compared to illustrate the velocity contours of both the conventional and modified ASWT. These contours represent the calculated average velocity fields of the overall flow at an inlet velocity of 8 m/s. With the addition of vortex generators, an increase in velocity is observed. The presence of the vortex generators enhances the output power and effectively reduces flow separation, allowing the turbine blades to capture energy more efficiently. The blue region in the figure represents a very low-velocity region and the red represents a high-velocity region.

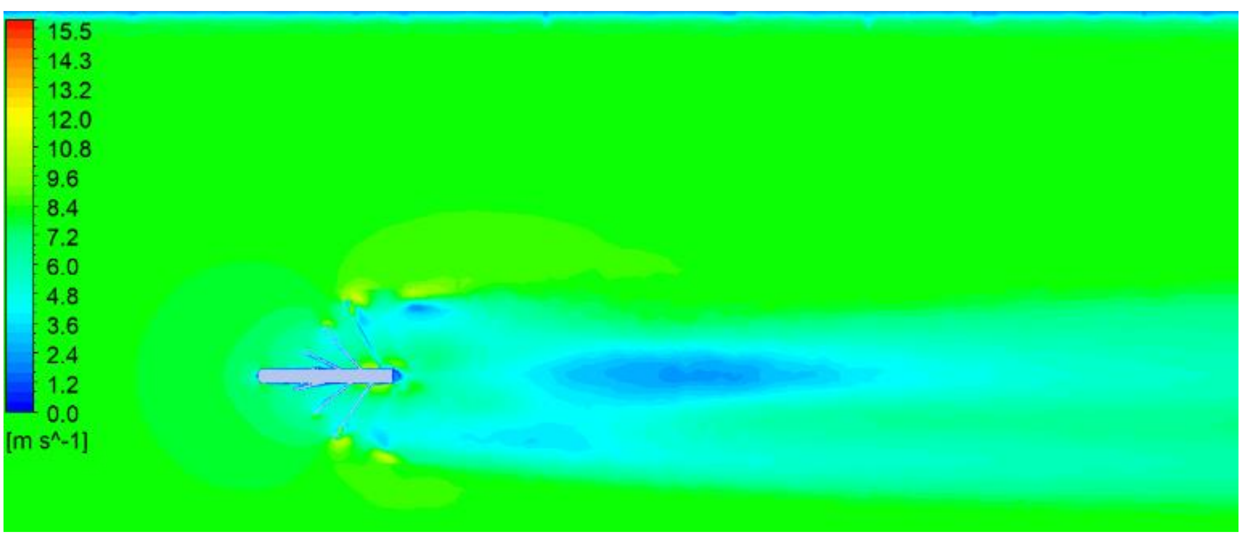

Figure 15: Conventional ASWT Velocity Contours at TSR of 2

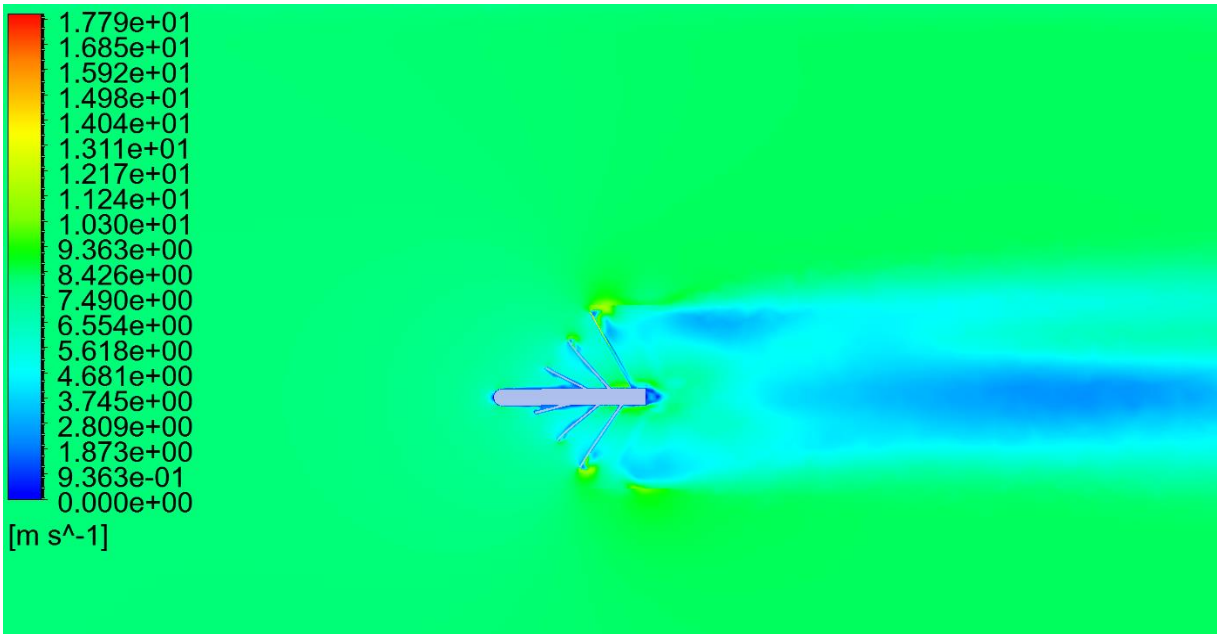

Figure 16: Modified ASWT Velocity Contours at TSR of 2

The comparison of Figure 17 and Figure 18 illustrates the different static pressure values of the conventional and modified Archimedes spiral wind turbine. With the addition of vortex generators, an increase in static pressure is observed. The primary purpose of vortex generators is to enhance aerodynamics; thus, improved flow dynamics lead to greater pressure difference. Based on these results, it can be concluded that incorporating vortex generators enhances output power. Both the conventional and modified turbines have similar contours; however, the modified turbine experiences a higher-pressure difference towards the front of the turbine. A higher-pressure difference indicates that the rotor extracts more energy from the wind, furthermore, leading to a higher power output. Additionally, the modified ASWT has a lower pressure region, suggesting improved flow attachment and extended adherence to the blade surface. The red contour represents a high pressure region and the blue represents a low pressure region.

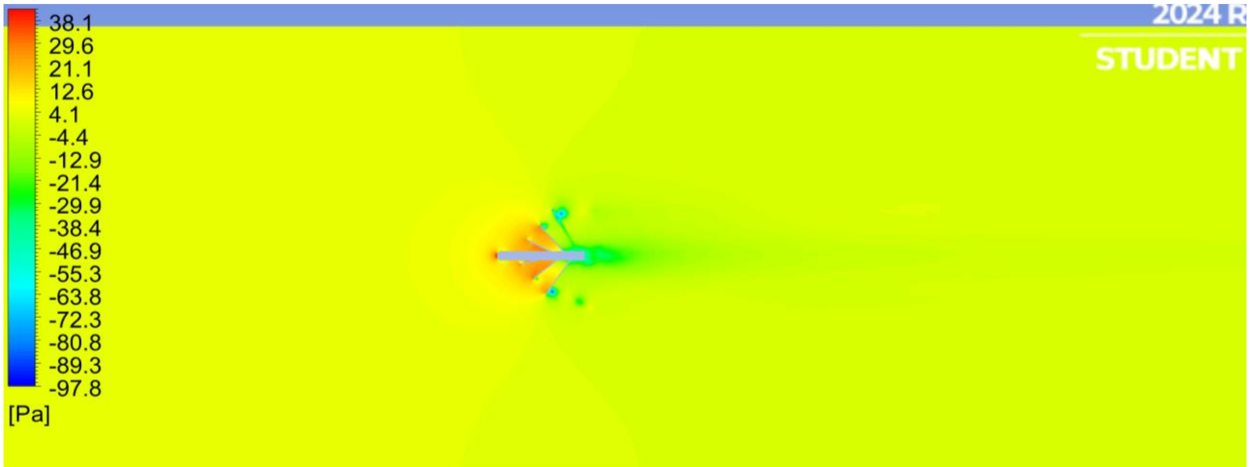

Figure 17: ASWT Static Pressure Contours at TSR of 2

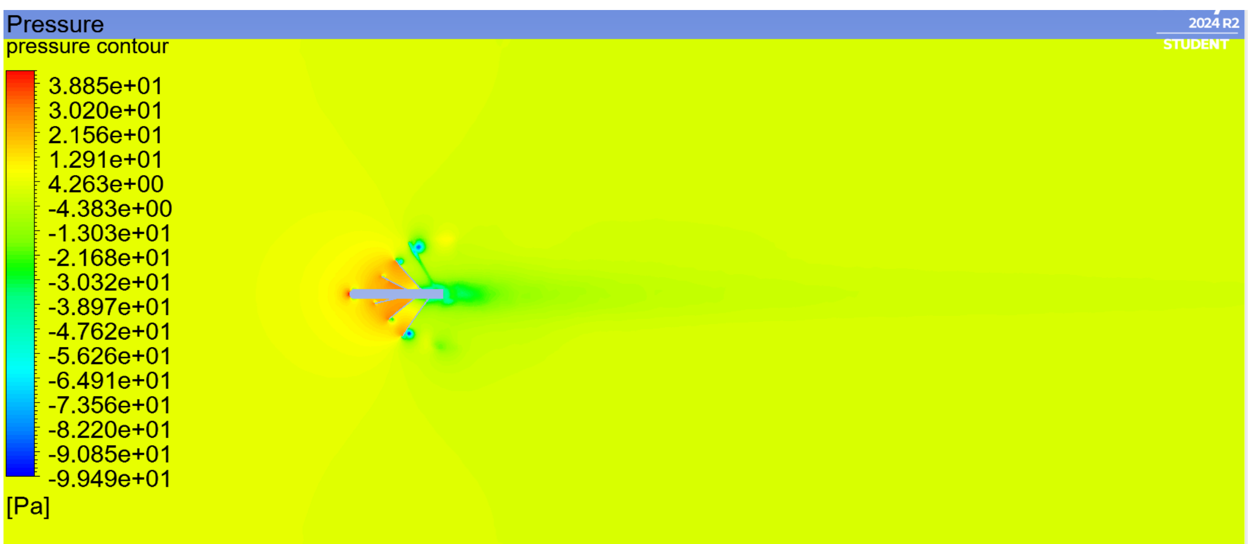

Figure 18: Modified ASWT Static Pressure Contours at TSR of 2

Figure 19 and Figure 20 provides a close-up view of the vortex generator in ANSYS. Near the vortex generators, low velocity is observed, indicating that as the ASWT rotates, there is a buildup of high pressure in the vicinity of the generators. The vortex generators create small vortices that energize the boundary layer, which helps prevent flow separation downstream. Consequently, the presence of a vortex generator is expected to slow down the airflow immediately around it. As shown in Figure 20, the path line in the vortex generators suggests that the VG is in fact delaying the flow separation and enhancing mixing in the boundary layer.

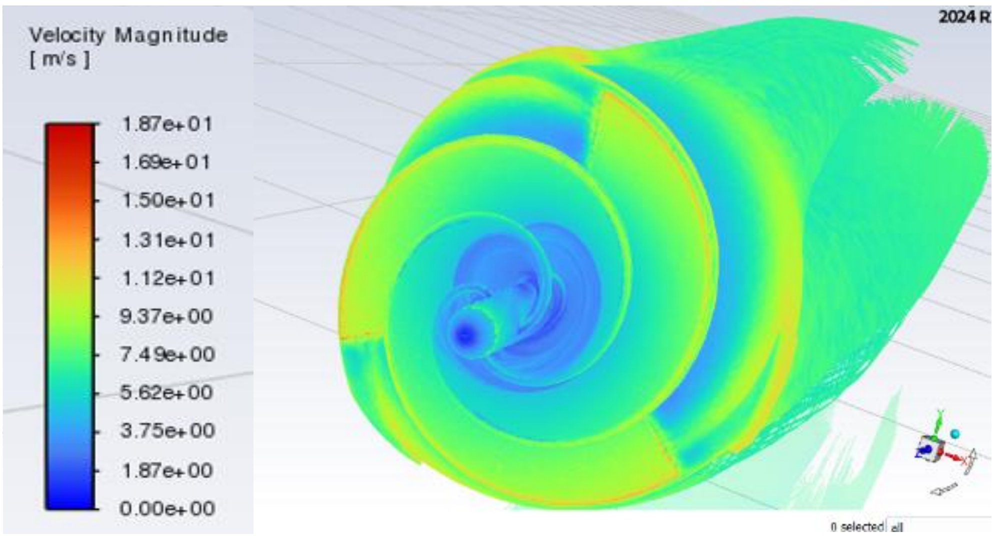

Figure 19: Close-up View of Modified ASWT

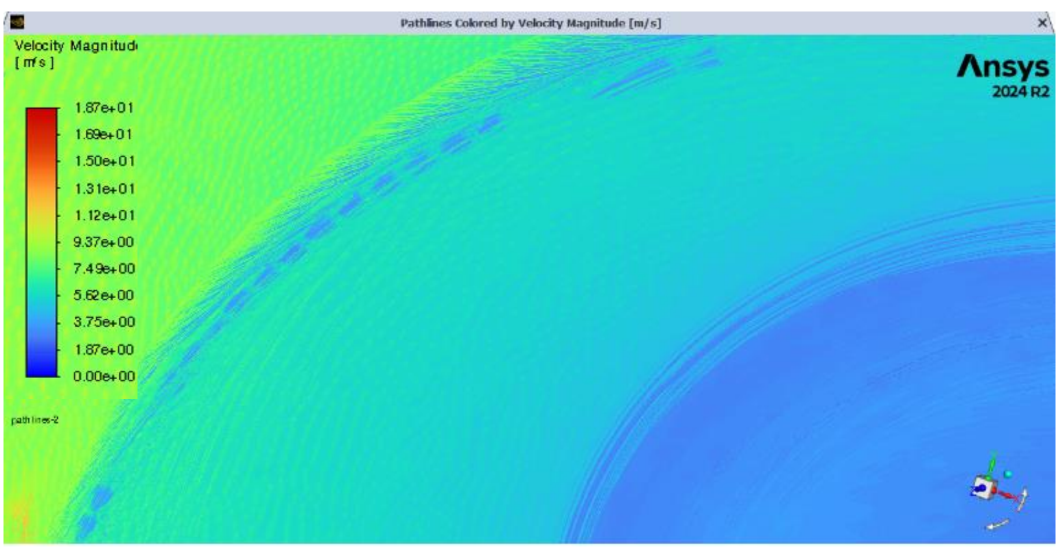

Figure 20: Modified ASWT Velocity Contour

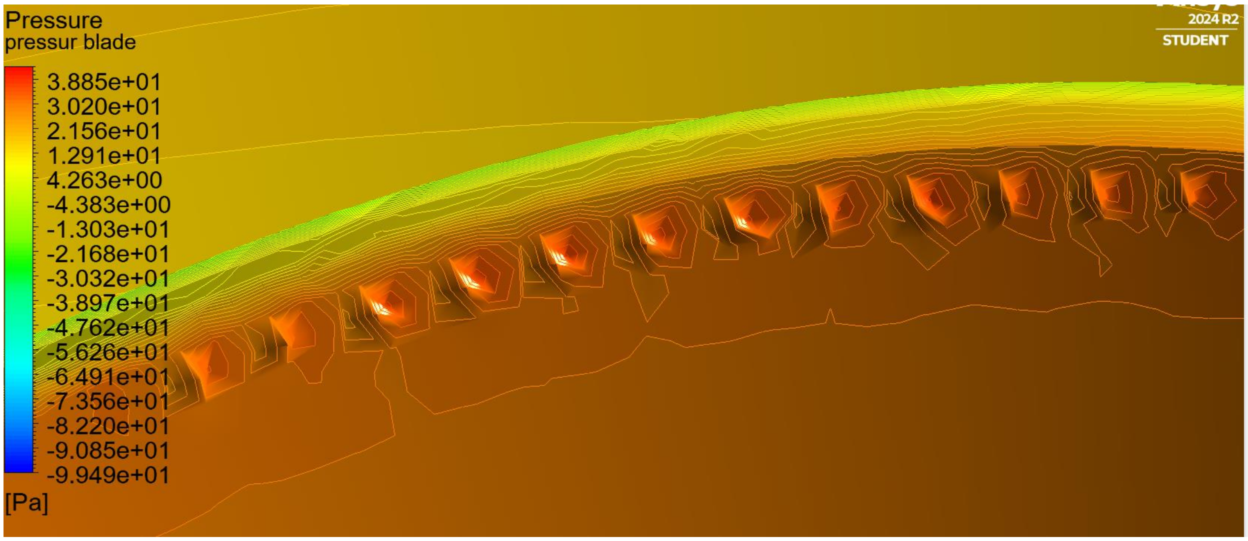

Figure 21: Pressure on Modified ASWT Blade

Figure 21 shows a localized high-pressure region at the leading edge of the vortex generators. This indicates the formation of strong vortices that help energize the boundary layer. The pressure gradient near the vortex generators indicates the effectiveness of the vortex formation to help delay the separation. In Figure 22 below, the front view of the modified ASWT illustrates the contours with the cross-section taken about the XY plane in the ASYS coordinate system. Behind the vortex generators, higher pressure regions are observed compared to the ASWT without the vortex generators. This indicates that the vortex generators are positively influencing the ASWT blades.

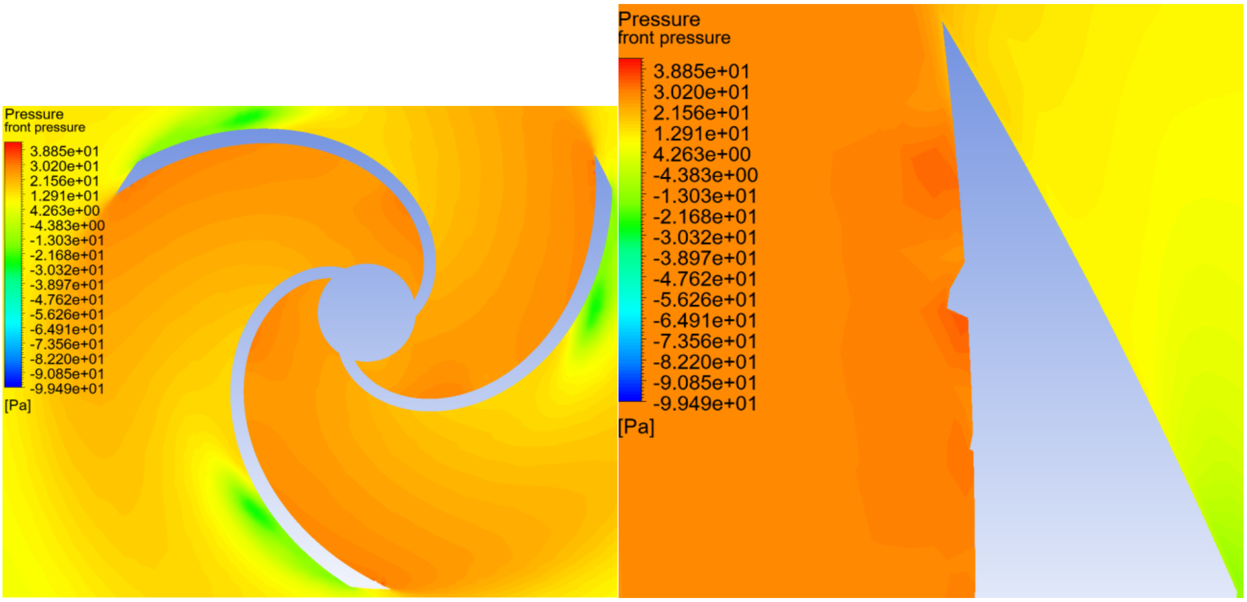

Figure 22: Front View of Modified ASWT

3.4 Experiment

3.4.1 Setup

The experiments were conducted at the University of Oklahoma Mechanical Engineering Lab. Figure 23 displays the wind tunnel that was utilized in the experiment and Figure 24 shows the close-up view of the test section where the ASWT will be attached and tested. The motor is from Baldor Standard-efficient industrial motor and is located towards the left of the wind tunnel. The wind starts from the right and moves towards the left of the wind tunnel and was set to wind speed ranging from 1-4 m/s.

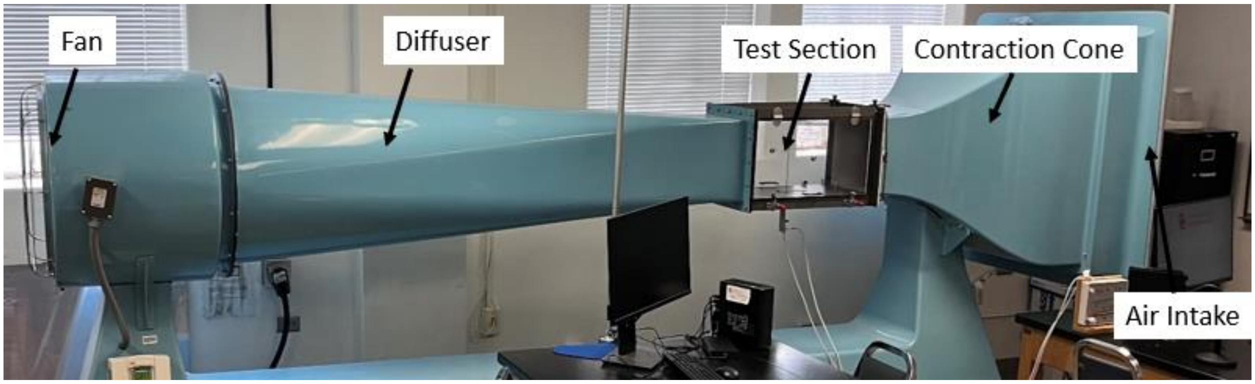

Figure 23: Wind Tunnel

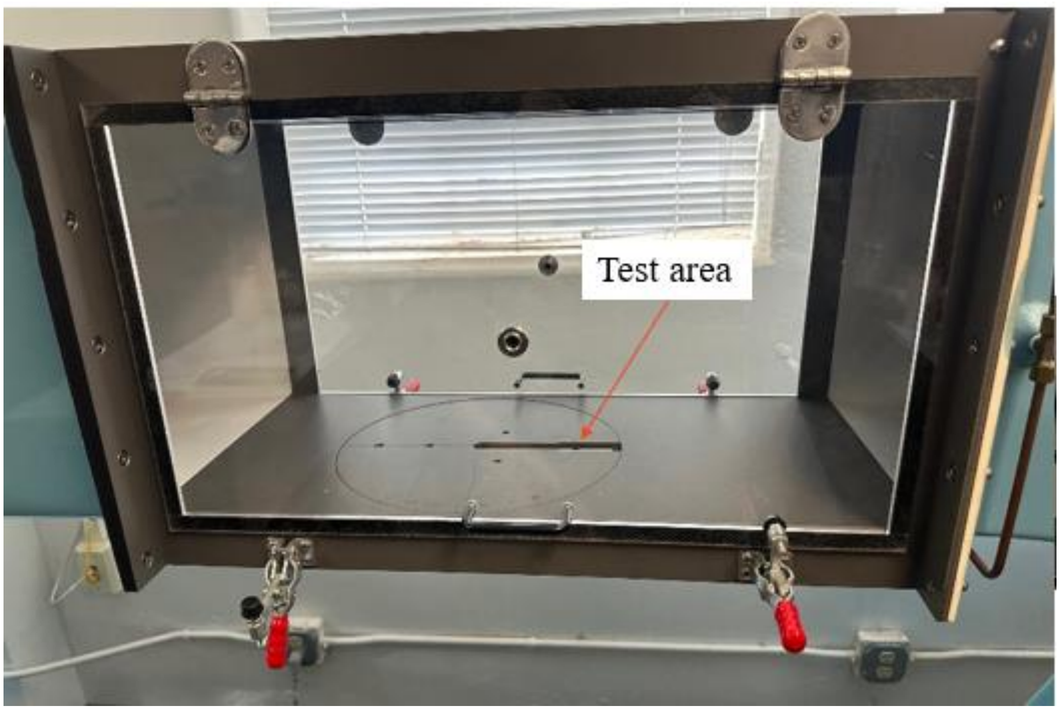

Figure 24: Test Section of Wind Tunnel

As shown in Figure 25, an adaptive mount was designed to properly hold the turbine in place. Before cutting the metal into the shape of the proposed design, a prototype of the design was printed in PLA. This step ensured proper fitting and sizing before using more expensive material and producing unnecessary waste. The prototype mount demonstrated good alignment and was able to properly fit the ASWT.

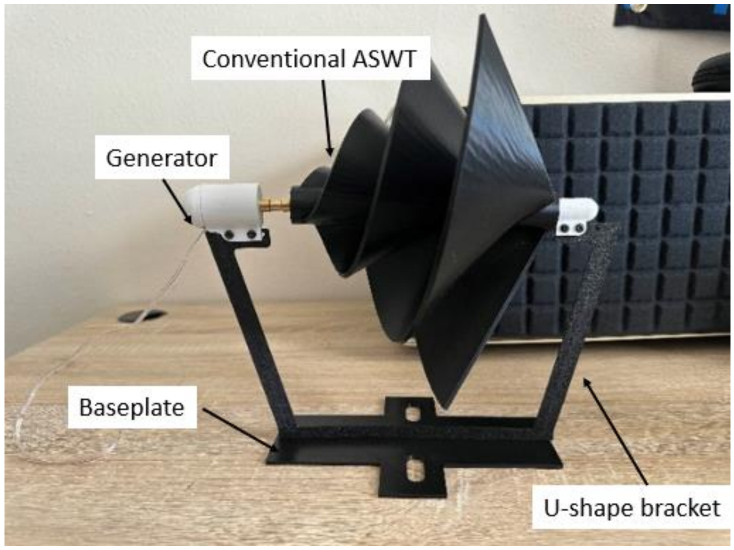

Figure 25: Prototype of Mount With ASWT

3.4.2 Manufacturing

Taking the design and parameters from Figure 5, the turbine was created using 3D printing technology with polylactide (PLA) material. The SolidWorks file was converted into a .STL to be sliced through the Bambu A1 software. Figure 26 shows the 3D printer in the process of manufacturing the ASWT and Figure 27 shows the slicer and support settings to print the ASWT. A 0.2 mm nozzle was used to enable precise printing of the vortex generators onto the turbine blades. As shown in the figure below, support was added to ensure high quality and precise prints. Through the manufacturing process, it was found that without supports, the abrupt movement of the printer causes the print to be unstable as the heating bed moves in the y-direction, which causes instability and reduces overall print quality. Supports can be added automatically or manually to the print. This study opted for the manual Tree structure support to ensure a high success rate. The modified ASWT took 48 hours to complete to accurately print the small vortex generators.

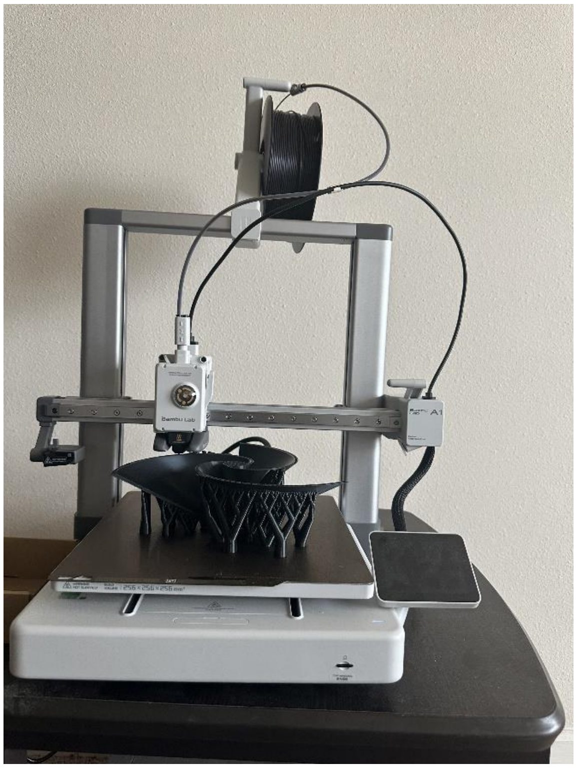

Figure 26: Bambu A1 With ASWT

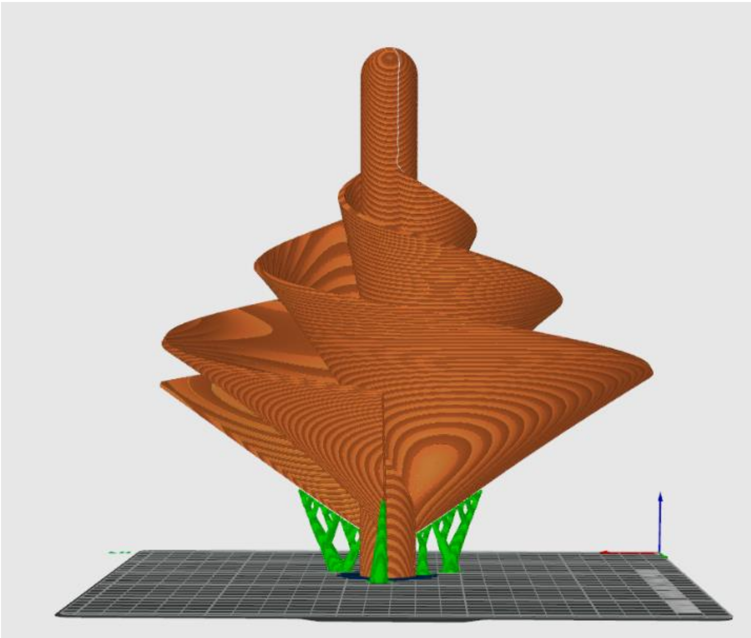

Figure 27: Bambu A1 Slicing Software

To secure the turbine in the wind tunnel, a base plate and a U-shape bracket were designed to hold the turbine in place. Figure 28 shows the U-shape bracket design and baseplate. The design constraint was that the assembly had to fit within a 1x1x2-foot box with 2 inches of clearance. The left of the figure shows the baseplate, which is designed to fasten securely to the base of the wind tunnel section. The hole in the baseplate is to insert a bolt with a washer and a nut on both sides.

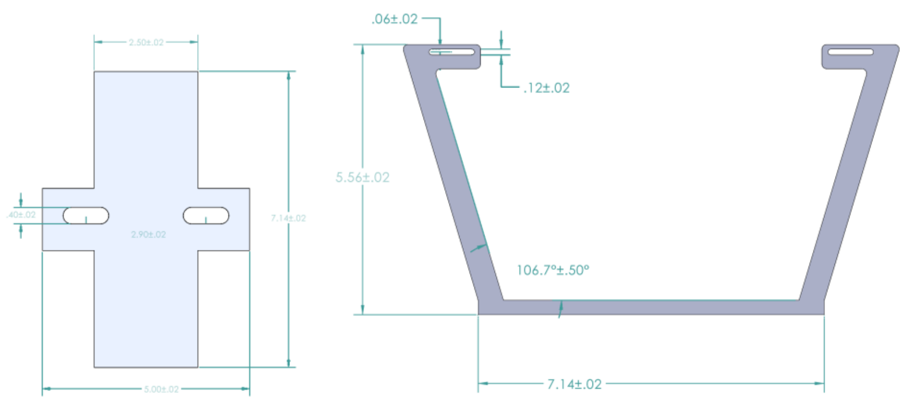

Figure 28: Dimension of ASWT Mount

The baseplate and the U-shape bracket are made from steel with a thickness of 0.07 inches and welded together to ensure durability in wind tunnel testing. The metal was cut using a water jet to ensure precise measurement for thin metals. Once it was machined, it was placed inside the wind tunnel, as seen in Figure 29. The mount is placed in the center of the wind tunnel and has about 1 inch of clearance on both the top and bottom of the ASWT.

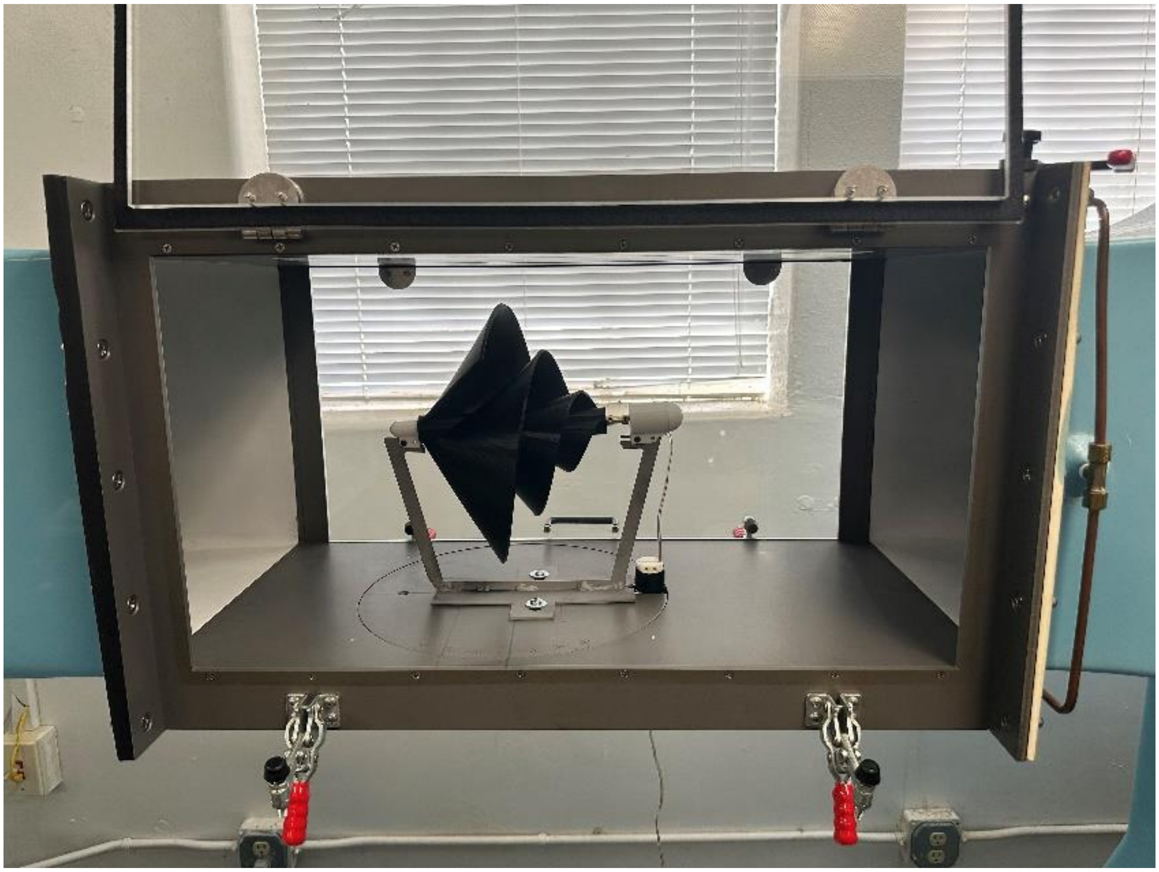

Figure 29: Fully Configured ASWT Experiment

3.4.3 Measuring Instrumentation

This experiment utilizes a tachometer, a 10W generator, INA226 Module, and Arduino Uno. The 10W generator is used to produce electrical power from the turbine, the INA226 measures the voltage and the current output from the generator, and the Arduino Uno processes and records the data collected in real-time. The tachometer is used to measure the rotation per minute (RPM) outside of the wind tunnel. A white line is marked on the ASWT to utilize the tachometer. Figure 30 illustrates the data collection setup, including wiring and connections.

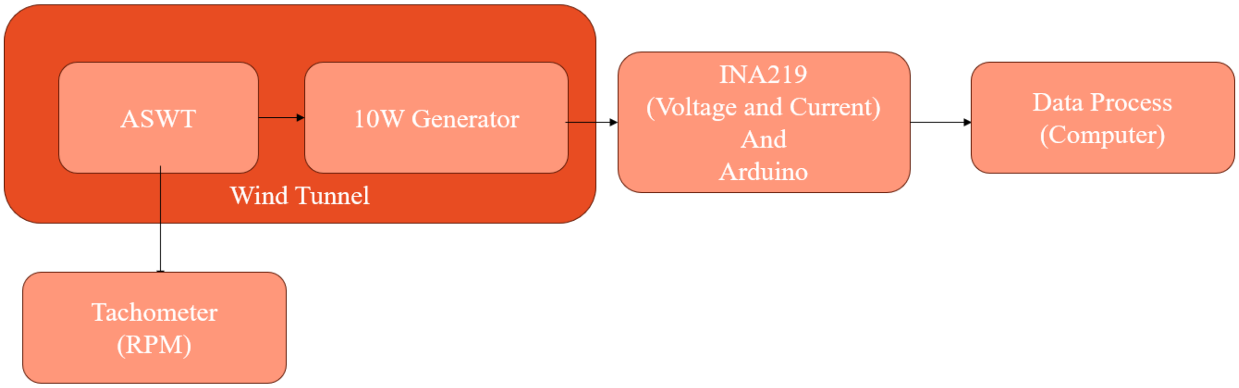

Figure 30: Measuring Process

To set up the data acquisition, Figure 31 shows the wire and hardware connection that was used in this study. The measured values are displayed on a laptop and can be extracted to Excel for analysis. The left image shows the Arduino Uno, INA219, capacitor, and resistor. A capacitor is added to decouple the motor from the power supply and to protect against inductive spikes [26]. The INA226 is rated to measure up to +26VDC and ±3.2 Amps with the resolution range of 0.8mA [26].

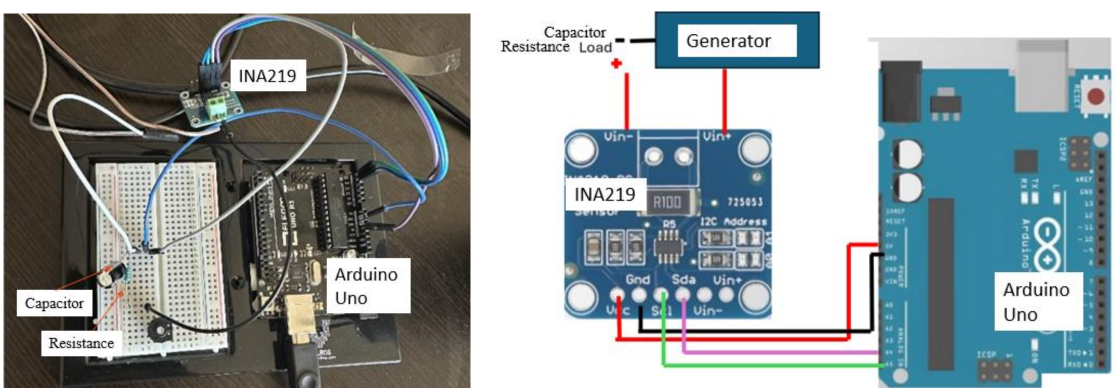

Figure 31: Data collection setup [27]

3.5 Results

3.5.1 Simulation

After determining the vortex generator size and placement, the CFD Ansys Fluent simulation yielded an improvement over the unmodified ASWT. TSR (λ) values have been used to find the values of the power coefficient (C_P) and torque coefficient(C_T). To calculate the power coefficient (C_P) and torque coefficient(C_T), the following equations are used: Eq. 11 and Eq. 12 [16].

$$\lambda = \frac{\omega r}{V} \tag{10}$$

where ω represents the angular velocity of the turbine, r represents the radius of the turbine, and the V Represents the inlet velocity of the stream in m/s. The formula for C_P is shown below

$$C_P = 2\frac{T\omega}{(\rho A V^3)} \tag{11}$$

T represents the torque of the turbine, ρ represents the air density, A represents the area of the turbine.

$$C_T = 4\frac{T}{(\rho A V^2 D)} \tag{12}$$

In the above equation (Eq. 12), D represents the diameter of the turbine. In Figure 32, the results are plotted to compare C_T vs. TSR at 8 m/s inlet wind velocity. The maximum coefficient of torque was observed at TSR 0.5 for both ASWT models. Both models exhibit a decrease in C_T as TSR increases, this is due to the fact that the turbine is rotating more relative to the incoming wind speed.

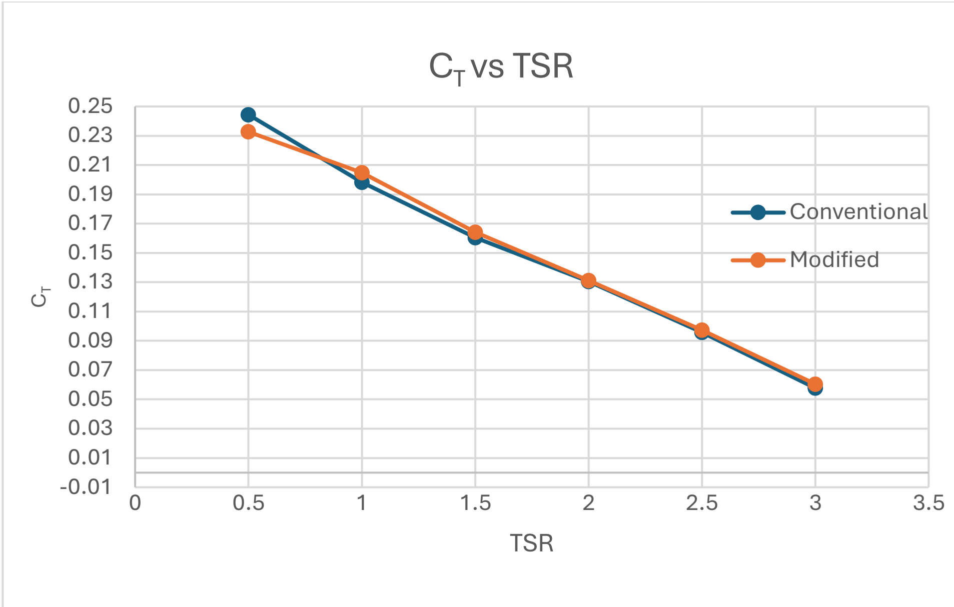

Figure 32: Tip Speed Ratio vs Torque Coefficient

In Figure 33, we observe that the maximum coefficient of power occurs at a Tip Speed Ratio (TSR) of 2 with an inlet velocity of 8 m/s. This indicates that the ASWT operates efficiently at low speeds. Furthermore, the addition of a vortex generator to the ASWT enhances its performance compared to the conventional ASWT. This comparison demonstrates that the vortex generators have a positive effect on the coefficient of torque. A higher C_P on the modified turbine indicates that the turbine is generating more rotational force than the conventional turbine at the same inlet wind velocity of 8 m/s.

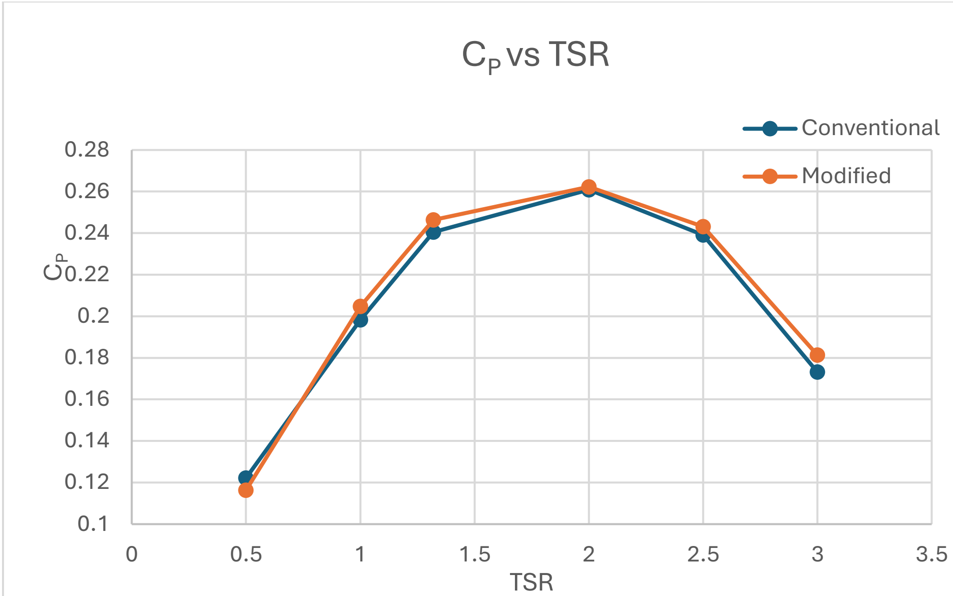

Figure 33: Tip Speed Ratio vs. Power Coefficient

These results showed that the implementation of vortex generators did positively impact the power output and performed better as TSR increased. As evident in Figure 32, the modified turbine begins with a lower performance value compared to the conventional turbine. This is primarily because the initial flow disturbances are caused by the vortex generators. However, as the Tip Speed Ratio (TSR) increases, the vortex generators help improve flow attachment. This results in a crossover point between TSR 0.5 and TSR 1. It can also be observed that the improvements from the vortex generators increase as TSR rises, as shown in Figure 33. A higher Cp in the modified turbine indicates that more energy can be output for a given wind speed. A similar scenario can be found in Moon's research [11]. By this comparison, the addition of vortex generators has a higher capability to capture more energy at higher wind speeds.

3.5.2 Experimental

The wind tunnel has been calibrated by the University of Oklahoma Wind Tunnel Lab, and data have been provided for this research. Table 5 shows the correlated wind speed of the wind tunnel at the input frequency. The exponential growth equation is given below,

$$y = A \cdot e^{kx} \tag{13}$$

where y is the output, A is the initial value, k represents the growth, e represents the Euler's number and x is the input. The output would calculate the velocity of the wind speed in the wind tunnel and the input is the frequency of which adjust the fan speed in the wind tunnel.

Table 5: Wind speed at input frequency

Frequency (Hz)	**Velocity (m/s)**
6	1.7882
8	1.9638
10	2.1567
12	2.3685
14	2.6011
16	2.8565
18	3.1371
20	3.4451
22	3.7835
24	4.1551

After the correlated wind speed were calculated, the experiment was conducted at frequency of 6, 8, 10, 12, 14, 16, 18, 20, 22, and 24 Hz. After the data has been retrieved from the ASWT, it utilized the electrical power equation to calculate the power output.

$$P = V * I \tag{14}$$

The V represents the voltage, and I represents the current that were collected through the INA219 sensor. The calculated power output was then compared between the conventional and modified values. As seen in Figure 34, the conventional performs better than the modified at 6 and 8 Hz by a very small margin. At 14 Hz, the difference becomes more noticeable, with the modified ASWT outperforming the conventional, and the biggest difference is seen at 22 Hz. Due to the nature of experiments, the values collected are lower than in simulations because it is in non-ideal conditions. External factors, such as electrical loss and heat loss, can affect the output of the data.

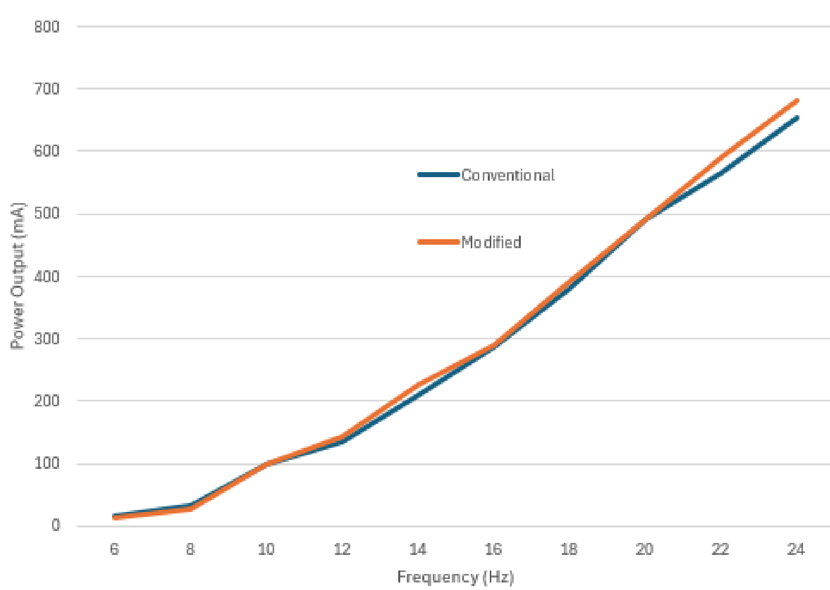

Figure 34: Power Output (mA) at Different Frequencies

The rotational velocity was recorded at the tested frequencies with the use of a tachometer. Table 6 list the measured rpm for both the modified and conventional ASWT at their respective frequency.

Table 6: Measured RPM at Different Frequencies

Frequency (Hz)	**Conventional**	**Modified**
6	475	475
8	850	843
10	1245	1253
12	1520	1560
14	1867	1921
16	2211	2259
18	2540	2593
20	2826	2863
22	3100	3137
24	3348	3390

From the table above, as the value of frequency increases, the measured RPM also increases. This is because when the frequency is increased, the wind speed increases as well and has an increasing force on the blades. The highest measured RPM was at 24 Hz with 3390 RPM. At low frequency, the conventional RPM is higher than the modified. This is due to the VGs introducing initial vorticity disturbances at low speeds.

3.6 Conclusion

The ASWT with vortex generators represents an innovative design through comprehensive design, modeling, and simulation analysis. Our findings for the simulation indicate that incorporating vortex generators led to power output increases of -4.9%, 3.3%, 2.4%, 0.5%, 1.7%, and 4.7% at Tip Speed Ratios (TSR) of 0.5, 1.0, 1.5, 2.0, 2.5, and 3, respectively. This suggests that the addition of vortex generators enhances performance at higher TSRs and surpasses the performance of the conventional ASWT. The highest coefficient of power was achieved at a TSR of 2, corresponding to a wind velocity of 8m/s. Experimental validation was also conducted with the use of a wind tunnel. The experiment was conducted at input frequencies of 6, 8, 10, 12, 14, 16, 18, 20, 22, and 24 Hz with the resulting output changes of -12.5%, -12.5%, 0%, 6.1%, 7.0%, 0.6%, 2.3%, 0.2%, 4.2%, 4.2% respectively. Furthermore, we have determined the size of vortex generators to improve flow attachment and reduce unwanted drag forces. For the future work of this research, experimental validation should be conducted outside of the wind tunnel for non-ideal conditions, such as natural wind speed variability, wind angle of attack, and turbulence. A more detailed investigation into the placement of vortex generators may be necessary to identify the optimal positions. Additionally, the potential effects of increasing or decreasing the number of vortex generators on the turbine should be explored. Future studies should also explore optimal vortex generator dimensions through formal optimization methods.

Chapter 4 Results and Discussion

A study on the sizing of large vortex generators (VGs) was conducted to evaluate their effect on ASWT, as shown in Figure 35. The results showed an increase in pressure when compared to both the smaller vortex generator and the conventional ASWT. However, the power output for the larger vortex generator was lower than that of both the smaller vortex generator and the conventional ASWT.

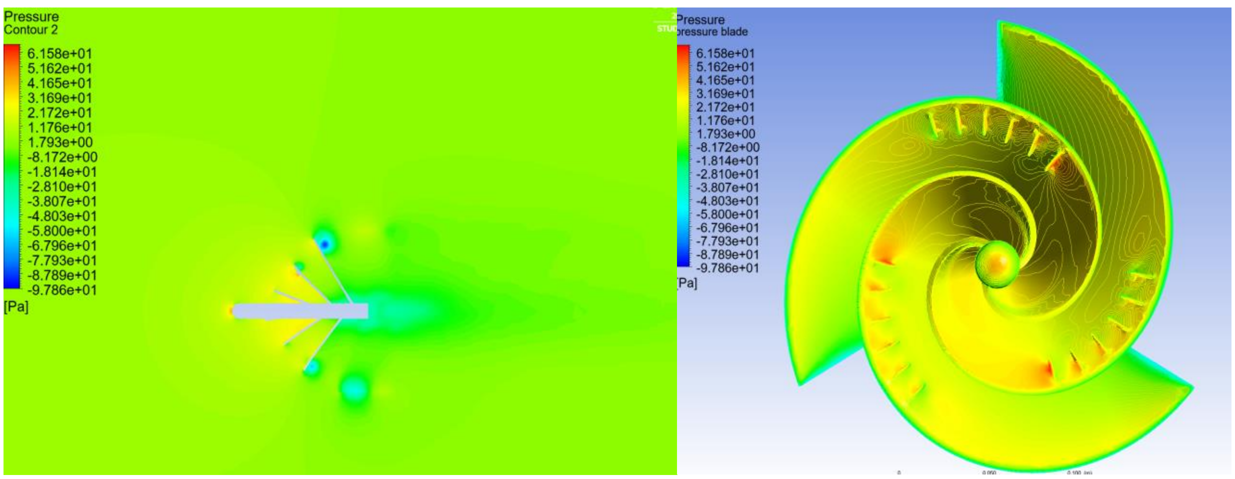

Figure 35: Pressure Contour of Large Vortex Generators

A comparison of the conventional ASWT, small VG, and large VG has been conducted. With the large VG, a decrease in performance was found, 5.5% and 6.2% when compared to conventional and small VG, respectively. The decrease in power output is due to the VG being too big and creating unwanted drag on the ASWT. The percentage decrease in performance was calculated using the following equation

$$Percent\ Decrease = \left(\frac{Original\ Value - Large\ VG\ value}{Original\ Value}\right) x\ 100 \qquad (15)$$

Table 7: Power Output Comparison

	Conventional	Small VG	Large VG
Power Output	4.01	4.04	3.79

Table 7 compares the power output of the different models. The model with the small vortex generator performed slightly better than the conventional. The large vortex generator performed the worst when compared to the other models. In Figure 36, the velocity contour is displayed with the larger vortex generators. Low-velocity regions can be observed on top of the large VGs.

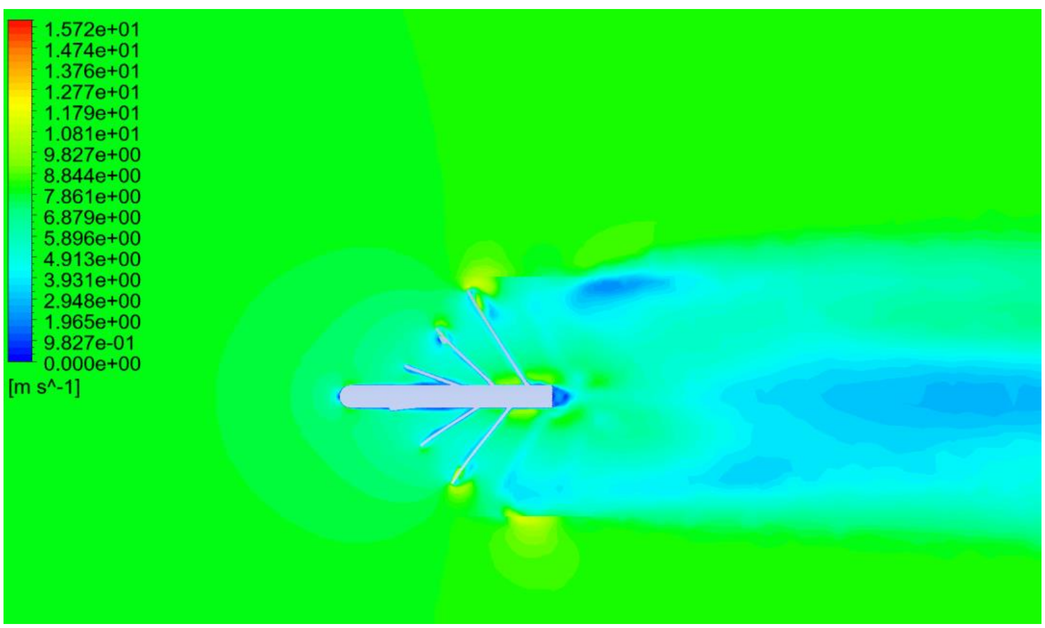

Figure 36: Velocity contour of large vortex generators

In the ANSYS Fluent solution, a path line visualization is set to see the area of interest. As the turbine is rotating about the -Z axis, the pressure is the highest at the very first vortex generator.

There are noticeably low-pressure regions behind the vortex generators and the leading edge of the turbine. However, it was found that the bigger vortex introduces excessive drag and reduces the power output of the ASWT. In Figure 37, the pressure was higher than the other sizes and the disturbances were prominent. Because of this reason, the sizing of this vortex generator was not used in further simulation and experiment.

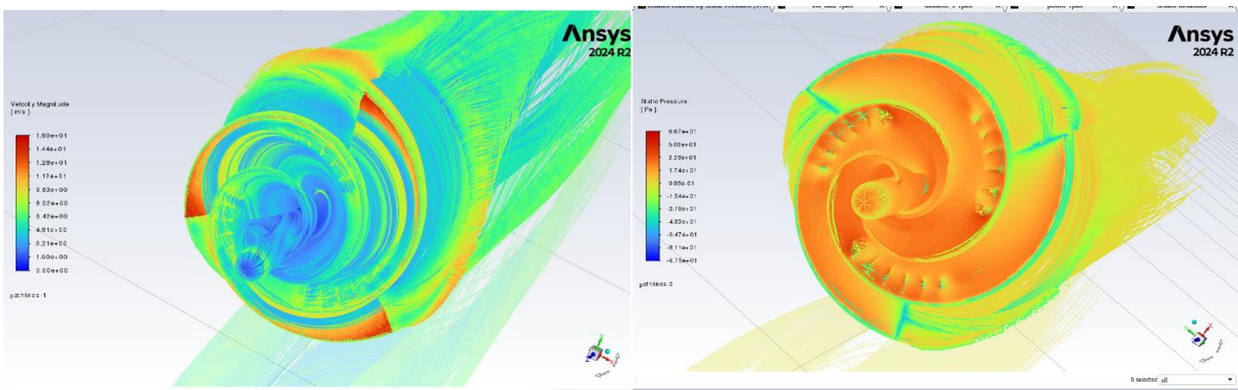

Figure 37: Velocity and Pressure path lines of ASWT with Large VG

In Chapter 3, it was discussed that once the vortex generator's dimensions and placement were finalized, a CFD Ansys Fluent simulation revealed that the modified Archimedes Spiral Wind Turbine (ASWT) outperformed its unmodified counterpart. To quantify this improvement, the Power Coefficient and Torque Coefficient were calculated using standard formulas (Equations 8 and 9). Various TSR values were tested to capture how changes in rotor speed relative to wind velocity influence these performance metrics.

Figure 31 compares the torque coefficients at an 8 m/s wind speed. Both turbines achieve their highest torque coefficient around a TSR of 0.5 and then show a gradual decline in C_T as TSR increases, reflecting the typical reduction in thrust when the rotor spins faster than the incoming wind. Figure 32 similarly plots the relationship between TSR and torque coefficient.

Meanwhile, Figure 33 indicates that the maximum power coefficient occurs at a TSR of 2. This suggests that the ASWT design, especially when equipped with vortex generators, operates more efficiently at relatively low wind speeds. Initially, the modified turbine exhibited slightly lower performance, due to initial flow disturbances introduced by the vortex generators. However, as TSR increases, these same vortex generators enhance flow attachment, causing the modified turbine to surpass the conventional design somewhere between TSR 0.5 and 1. Beyond that crossover point, the performance gap continues to widen in favor of the modified turbine. These findings confirm that adding vortex generators can positively affect output power and torque, especially at higher wind speeds. Similar outcomes have been reported in Moon's research [11] underscoring the importance of vortex generators in improving energy capture capabilities in small wind turbine designs.

The ASWT design of both the conventional and the modified model was tested at the University of Oklahoma Wind Tunnel Lab. Chapter 3 discussed the setup of the experiment and the adaptive mount that was designed for the experiment. The process of conducting the experiment is shown in Figure 30 and the data setup is shown in Figure 31. Power output and rotational speed data were collected for the frequencies at 6, 8, 10, 12, 14, 16, 18, 20, 22, and 24 Hz. As the frequency increases, the RPM also increases. This is due to the blades experiencing more external force and causing the turbines to rotate faster. The frequency was then converted to wind speed in m/s, where the correlation was found to be exponential. In Figure 34, the experiment showed that at lower frequencies, the conventional model performed better than the modified model; however, after a frequency of 12 Hz, it was found that the modified ASWT performed better than the conventional ASWT.

Chapter 5 Conclusion and Future Scope

5.1 Conclusion

In this work, it was found that the initial Dynamic mesh method was not appropriate for this research. The research focused on the overall output of the ASWT with and without the vortex generators, therefore mesh movement was not necessary. Not only was the method not necessary for this case, but it was also very computationally heavy and required long hours to simulate.

The study of large vortex generators was conducted to see the ASWT performance compared to that of the conventional and small vortex generators. It was found that at TSR 2 and wind speed of 8 m/s, the large vortex generators had a negative impact on their performance. The large vortex generator showed a decrease in performance of 5.5% and 6.2% when compared to conventional and small VG respectively. In conclusion, the large vortex generator of this size is not recommended due to the excessive drag it creates.

The final VGs design and placement were finalized in Chapter 3. The Archimedes Spiral Wind Turbine (ASWT) equipped with vortex generators represents the integrated design, modeling, and simulation process. Results show that adding vortex generators produced power output changes of –4.9%, 3.3%, 2.4%, 0.5%, 1.7%, and 4.7% at TSRs of 0.5, 1.0, 1.5, 2.0, 2.5, and 3, respectively. Notably, performance gains were more pronounced at higher TSRs, indicating that the modified turbine surpasses the unmodified ASWT in these operating regions. Moreover, optimizing vortex generator dimensions helped maintain airflow attachment while mitigating drag forces, with the turbine's peak power coefficient reached at a TSR of 2 at an 8 m/s wind speed.

Chapter 3 also mentions the experimental work that was conducted, as well as the findings. The turbine was designed and manufactured for both the modified and conventional ASWT. The

ASWT was printed with PLA material. The mount to hold the turbine inside the wind tunnel was also prototyped and machined with steel to maintain proper strength. Experiments were conducted for both modified and conventional models by following the same procedure. The experiment found that at frequency of 6, 8, 10, 12, 14, 16, 18, 20, 22, and 24 with the output increase of -12.5%, -12.5%, 0%, 6.1%, 7.0%, 0.6%, 2.3%, 0.2%, 4.2%, 4.2% respectively. These frequencies are then calibrated to the respective wind speed that ranges from 1-4 m/s and represent low wind conditions that the turbine may experience.

5.2 Future Work

In this research, the focus was on the vortex generators' effect on Archimedes' spiral wind turbine. In addition to studying the effect of VGs on ASWT, one could look further into optimization of the vortex generators sizing and placement on ASWT. By optimizing the placement and sizing, an increase in performance could be found and further improve the ASWT performance.

This research also utilized ANSYS Fluent with the turbulence model SST k-ω. In the future, when better turbulence models are created to accurately capture the flow, they can be utilized through different software. Different software can be used to compare the accuracy of the performance of ASWT, such as ANSYS Commercial and Star-CCM+. The advantage of using an ANSYS commercial is that it supports unlimited core usage for parallel, meaning that it can solve complex problems more quickly and effectively.

References

[1] Intergovernmmental Panel on Climate Change, Climate Change 2021: the Physical Science Basis. Contribution of Working Group I to the Sixth Assessment Report of the IPCC, V. Masson-Delmotte et al., Eds. Cambridge, UK.: Cambridge University Press, 2021

[2] Genç, Mustafa Serdar, et al. "Flow characteristics over NACA4412 airfoil at low Reynolds number." EPJ web of conferences. Vol. 114. EDP Sciences, 2016.

[3] Tummala, Abhishiktha & Velamati, Ratna Kishore & Sinha, Dipankur & Indraja, V. & Krishna, V. (2016). A review on small scale wind turbines. Renewable and Sustainable Energy Reviews. 56. 1351-1371. 10.1016/j.rser.2015.12.027.

[4] American Bird Conservancy, “Wind Energy and Birds.” [Online]. Available: https://abcbirds.org/program/wind-energy-and-birds/

[5] Herraprastanti, Eva & Saputro, Widianto. (2021). Simulation of Opening Angle of Archimedes Wind Turbine Design Based on the Fibonacci Series. International Journal of Engineering, Science and Information Technology. 2. 50-57. 10.52088/ijesty.v2i1.192.

[6] Sapkota, Sudip et al. “Design, CFD Analysis and Modelling of Archimedean-Spiral type Wind Turbine.” (2020).

[7] United States, Department of Energy. “How Do Wind Turbines Work?” Energy.gov,https://www.energy.gov/eere/wind/how-do-wind-turbines-work.U.S. Department of Energy, “How Do Wind Turbines Work?” *Energy.gov*. [Online]. Available: https://www.energy.gov/eere/wind/how-do-wind-turbines-work

[8] Froese, M. (2017, October 10). *Vortex generators boost wind turbine performance, AEP*. Windpower Engineering & Development. https://www.windpowerengineering.com/vortex-generators-boost-wind-turbine-performance-aep/

[9] Bahador Bakhtiari Nia, Mohammad Ja'fari, Adel Rezaei Ranjbar, Artur J. Jaworski,Passive control of boundary layer flow separation on a wind turbine airfoil using vortex generators and slot,OceanEngineering,Volume283,2023,115170,ISSN00298018,https://doi.org/10.1016/j.oceaneng.2023.115170

[10] Menter, F.R., et al., 2006. A Correlation-Based Transition Model Using Local Variables—Part I: Model Formulation.

[11] Moon, Hyeongi, et al. "Numerical and Experimental Validation of Vortex Generator Effect on Power Performance Improvement in MW-Class Wind Turbine Blade." Renewable Energy, vol. 212, 2023, pp. 443-454. ISSN 0960-1481, May 2024.J. Clerk Maxwell, A Treatise on Electricity and Magnetism, 3rd ed., vol. 2. Oxford: Clarendon, 1892, pp.68–73.

[12] Jiang, Ruifang, et al. "Numerical Study on the Influence of Vortex Generators on Wind Turbine Aerodynamic Performance Considering Rotational Effect." Renewable Energy, vol. 186, 2022, pp. 730-741. ISSN 0960-1481, https://doi.org/10.1016/j.renene.2022.01.026.Y. Yorozu, M.

[13] Hand, M. M., et al. Unsteady Aerodynamics Experiment Phase VI: Wind Tunnel Test Configurations and Available Data Campaigns.NREL/TP-500-29955, National Renewable Energy Laboratory, 200

[14] Im, H., Kim, S. & Kim, B. “Investigation of effective design and application of vortex generators for the wind turbine blades”. J Mech Sci Technol 39, 671–685 (2025). https://doi.org/10.1007/s12206-025-0114-8

[15] Zitti, Gianluca, et al. "Efficiency Evaluation of a Ductless Archimedes Turbine: Laboratory Experiments and Numerical Simulations." Renewable Energy, vol. 146, 2020, pp. 867-879,

[16] Nawar, Mohamed A. A., et al. "Experimental and Numerical Investigations of the Blade Design Effect on Archimedes Spiral Wind Turbine Performance." Energy, vol. 223, 2021, 120051,

[17] Abdel Hameed, Hossam S., et al. "Shape Optimization of a Shrouded Archimedean-Spiral Type Wind Turbine for Small-Scale Applications." Energy, vol. 263, part B, 2023, 125809,

[18] Sadrehaghighi, Ideen. (2022). Dynamic Meshing. 10.13140/RG.2.2.26505.31842.

[19] Alam, Firoz & Jin, Yingai. (2023). The Utilisation of Small Wind Turbines in Built-Up Areas: Prospects and Challenges. Wind. 3. 418-439. 10.3390/wind3040024.

[20] Xue, Sunjiahe Advanced Aerodynamic Modeling of Vortex Generators for Wind Turbine Applicationswww.researchgate.net/publication/289260092_Advanced_aerodynamic_modeling_of_vortex_generators_for_wind_turbine_applications.

[21] Yang, Y., Wang, D., Zhang, H., Zha, R., Wu, G., Cai, C., Zhang, J., & Li, Q. (2025). Enhancing Aerodynamic Performance of Horizontal Axis Wind Turbine Blade Aerodynamic Performance Under Rough Wall Condition Using Vortex Generators. *Journal of Marine Science and Engineering*, *13*(3), 397. https://doi.org/10.3390/jmse13030397

[22] Ebrahimi, Sahand & Ghassemi, Mohammad Aref. (2018). Numerical Aerodynamics Analysis of the of the Archimedes Screw Wind Turbine. ,” *Int. J. Multidiscip. Sci. Eng.*, 2018, pp. 12–15.

[23] Ozeh, M, Mishra, A, & Wang, X. "Mini Wind Turbine for Small Scale Power Generation and Storage (Archimedes Wind Turbine Model)." *Proceedings of the ASME 2018 International Mechanical Engineering Congress and Exposition*. *Volume 6B: Energy*.

Pittsburgh, Pennsylvania, USA. November 9–15, 2018. V06BT08A043. ASME. https://doi.org/10.1115/IMECE2018-88455

[24] Coughtrie, A. R., et al. "Effects of Turbulence Modelling on Prediction of Flow Characteristics in a Bench-Scale Anaerobic Gas-Lift Digester." Bioresource Technology, vol. 138, 2013, pp. 297-306,

[25] Sapkota, Sudip. “Design, CFD Analysis and Modelling of Archimedean-Spiral type Wind Turbine” IOE Conference, vol. 6, 2019, pp. 563 – 571.

[26] Adafruit Industries, “Adafruit INA219 Current Sensor Breakout,” *Adafruit Learning System*. Available: https://learn.adafruit.com/adafruit-ina219-current-sensor-breakout/wiring

[27] Rembor, Kaattni "Adafruit INA219 Current Sensor Breakout." Adafruit Learning System, Adafruit Industries, 22 Jan. 2025, learn.adafruit.com/adafruit-ina219-current-sensor-breakout.

Appendix A: Code

Code to collect data and save as CSV

```
import serial
import csv
ser = serial.Serial('COM4', 115200, timeout=1)
# Open CSV File
with open("arduino_data.csv", "w", newline="") as file:
    writer = csv.writer(file)
    # Read and discard the first line (CSV headers)
    ser.readline()

    # Write column headers
    writer.writerow(["Voltage (V)", "Current (mA)", "Power (mW)"])
    print("Recording data... Press Ctrl+C to stop.")
    try:
        while True:
            line = ser.readline().decode('utf-8').strip()
            if "," in line:
                data = line.split(", ")
                writer.writerow(data)
                print(line)
    except KeyboardInterrupt:
        print("\nRecording stopped. Data saved to arduino_data.csv")
        ser.close()
```

Code in the Arduino to read and write data from the ina219 sensor

```
#include <Wire.h>
#include <Adafruit_INA219.h>
Adafruit_INA219 ina219;
void setup() {
   Serial.begin(115200);
   if (!ina219.begin()) {
      Serial.println("Failed to find INA219 chip");
      while (1) { delay(10); }
   }
   Serial.println("INA219 sensor found!");
}
void loop() {
   float busVoltage = ina219.getBusVoltage_V();
   float current_mA = ina219.getCurrent_mA();
   float power_mW = ina219.getPower_mW();
 // Print data in CSV format
   Serial.print(busVoltage, 2); Serial.print(", ");  // Voltage
   Serial.print(current_mA, 1); Serial.print(", ");  // Current
   Serial.println(power_mW, 1);  // Power
   delay(1000);
}
```

MatLab code to calculate the calibration from frequency (Hz) to wind velocity

```
x = linspace(0, 45, 45);  % hz
y = 1.4148*exp(0.0458*x)
```